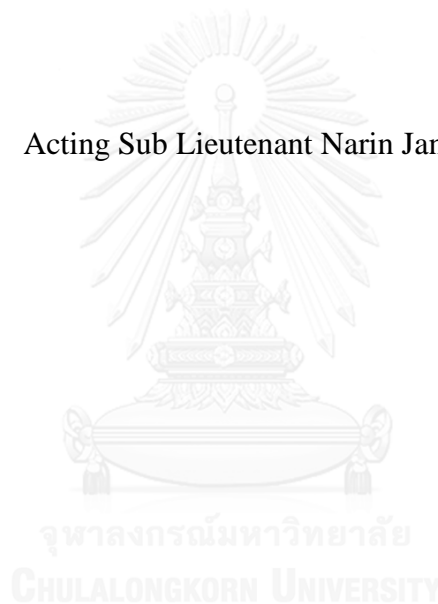


NANOSTRUCTURAL INVESTIGATION AND ENGINEERING OF
ELECTRODEPOSITED ZINC COATINGS AND THEIR CHROMIUM
AND GRAPHENE-BASED PASSIVATION LAYERS

Acting Sub Lieutenant Narin Jantaping



บทคัดย่อและแฟ้มข้อมูลฉบับเต็มของวิทยานิพนธ์ตั้งแต่ปีการศึกษา 2554 ที่ให้บริการในคลังปัญญาจุฬาฯ (CUIR)
เป็นแฟ้มข้อมูลของนิสิตเจ้าของวิทยานิพนธ์ ที่ส่งผ่านทางบัณฑิตวิทยาลัย

The abstract and full text of theses from the academic year 2011 in Chulalongkorn University Intellectual Repository (CUIR)
are the thesis authors' files submitted through the University Graduate School.

A Dissertation Submitted in Partial Fulfillment of the Requirements
for the Degree of Doctor of Philosophy Program in Nanoscience and Technology

(Interdisciplinary Program)

Graduate School

Chulalongkorn University

Academic Year 2016

Copyright of Chulalongkorn University

การวิเคราะห์และควบคุมโครงสร้างระดับนาโนของชั้นเคลือบสังกะสีที่ชุบด้วยไฟฟ้าและชั้นเคลือบ
พาสซีวชั้นโครเมียมและกราฟีน



วิทยานิพนธ์นี้เป็นส่วนหนึ่งของการศึกษาตามหลักสูตรปริญญาวิทยาศาสตรดุษฎีบัณฑิต
สาขาวิชาวิทยาศาสตร์นาโนและเทคโนโลยี (สหสาขาวิชา)

บัณฑิตวิทยาลัย จุฬาลงกรณ์มหาวิทยาลัย

ปีการศึกษา 2559

ลิขสิทธิ์ของจุฬาลงกรณ์มหาวิทยาลัย

Thesis Title	NANOSTRUCTURAL INVESTIGATION AND ENGINEERING OF ELECTRODEPOSITED ZINC COATINGS AND THEIR CHROMIUM AND GRAPHENE-BASED PASSIVATION LAYERS
By	Acting Sub Lieutenant Narin Jantaping
Field of Study	Nanoscience and Technology
Thesis Advisor	Associate Professor Dr. Yuttanant Boonyongmaneerat
Thesis Co-Advisor	Professor Dr. Christopher A.Schuh

Accepted by the Graduate School, Chulalongkorn University in Partial Fulfillment of the Requirements for the Doctoral Degree

..... Dean of the Graduate School
(Associate Professor Dr. Sunait Chutintaranond)

THESIS COMMITTEE

..... Chairman
(Associate Professor Dr. Vudhichai Parasuk)

..... Thesis Advisor
(Associate Professor Dr. Yuttanant Boonyongmaneerat)

..... Thesis Co-Advisor
(Professor Dr. Christopher A.Schuh)

..... Examiner
(Dr. Ratthapol Rangkupan)

..... Examiner
(Dr. Nadnudda Rodthongkum)

..... External Examiner
(Dr. Wannipha Amatyakul)

นรินทร์ จันทะพิงค์ : การวิเคราะห์และควบคุมโครงสร้างระดับนาโนของชั้นเคลือบสังกะสีที่ชุบด้วยไฟฟ้าและชั้นเคลือบพาสซีเวชันโครเมียมและกราฟีน (NANOSTRUCTURAL INVESTIGATION AND ENGINEERING OF ELECTRODEPOSITED ZINC COATINGS AND THEIR CHROMIUM AND GRAPHENE-BASED PASSIVATION LAYERS) อ.ที่ปรึกษาวิทยานิพนธ์หลัก: รศ. ดร. ยุทธนันท์ บุญยมณีนรัตน์, อ.ที่ปรึกษาวิทยานิพนธ์ร่วม: ศ. ดร. คริสโตเฟอร์ เอ.ซู, หน้า.

การชุบสังกะสีด้วยไฟฟ้าเป็นการเคลือบที่สำคัญและใช้กันอย่างแพร่หลายสำหรับการป้องกันการกัดกร่อนในการใช้งานต่างๆ อย่างไรก็ตามความเข้าใจเกี่ยวกับความสัมพันธ์ระหว่างกระบวนการผลิต โครงสร้างขนาดไมโคร/นาโน และคุณสมบัติของวัสดุมีค่อนข้างจำกัด วิทยานิพนธ์ฉบับนี้มีจุดมุ่งหมายเพื่อพัฒนากรอบความสัมพันธ์ด้านโครงสร้างและการกัดกร่อนของชั้นเคลือบสังกะสีและชั้นเคลือบโครเมียมที่ผ่านกระบวนการชุบด้วยไฟฟ้า และศึกษากระบวนการใหม่ โดยเฉพาะอย่างยิ่งการเคลือบด้วยกราฟีน ซึ่งจะสามารถป้องกันการกัดกร่อนของสังกะสีได้ งานวิจัยที่จัดทำขึ้นในวิทยานิพนธ์ฉบับนี้แบ่งออกเป็น 3 ส่วนคือ (1) ความสัมพันธ์ระหว่างกระบวนการผลิต โครงสร้างและสมบัติของชั้นเคลือบสังกะสีด้วยไฟฟ้า (2) ผลกระทบของโครงสร้างของชั้นเคลือบสังกะสีด้วยไฟฟ้าต่อการเกิดชั้นเคลือบพาสซีเวชันโครเมียมไตรวาเลนต์ และ (3) ความเป็นไปได้ของการเคลือบกราฟีนให้มีศักยภาพในการป้องกันการกัดกร่อน

กลุ่มชิ้นงานเคลือบสังกะสีที่ไม่ใช่โซลาร์เซลล์แบบต่างเป็นมิตรกับสิ่งแวดล้อม ทั้งที่มีและไม่มีเคลือบพาสซีเวชันโครเมียมไตรวาเลนต์ ถูกเตรียมโดยกระบวนการชุบเคลือบด้วยไฟฟ้า เพื่อตรวจสอบคุณสมบัติของโครงสร้างขนาดไมโคร/นาโน และคุณสมบัติการกัดกร่อน โดยใช้สารเติมแต่ง 3 กลุ่ม เพื่อปรับเปลี่ยนโครงสร้างของชั้นเคลือบสังกะสี จากการใช้เทคนิคการวิเคราะห์ลักษณะเฉพาะแบบสมัยใหม่ประกอบด้วย กล้องจุลทรรศน์อิเล็กตรอนแบบส่องกราด (FE-SEM), เทคนิคการเลี้ยวเบนของเอกซเรย์ (XRD), โฟกัสลำแสงไอออน (FIB) และกล้องจุลทรรศน์อิเล็กตรอนแบบส่องผ่าน (TEM) ได้พบว่าสารเติมแต่งมีบทบาทต่อการเรียงตัวของผลึกและข้อบกพร่องภายในชั้นเคลือบ และยังมีบทบาทสำคัญในการควบคุมพฤติกรรมกัดกร่อนของชั้นเคลือบ นอกจากนี้ เกลือโพลีควอเทอนารีเอมี เป็นสารเติมแต่งที่มีประสิทธิภาพสำหรับการชุบสังกะสี และส่งผลต่อการก่อตัวของเฟสผสมระหว่างออสเทนไนต์และออกไซด์ที่มีความหนาแน่นสูงมากในชั้นฟิล์มโครเมต ซึ่งทำให้มีความต้านทานต่อการกัดกร่อนสูง และสุดท้าย ได้ทำการศึกษาความเป็นไปได้ของการชุบเคลือบผิวด้วยกราฟีนเพื่อการกัดกร่อน พบว่า กราฟีนสามารถเคลือบลงบนพื้นผิวได้โดยใช้การชุบเคลือบด้วยไฟฟ้า โดยจะถูกควบคุมโดยสารเติมแต่ง ความหนาแน่นกระแส และระยะเวลาในการชุบ จากการเคลือบด้วยกราฟีนแสดงให้เห็นถึงผลการต้านทานการกัดกร่อนที่เป็นประโยชน์และทำให้มีแนวโน้มที่จะใช้สำหรับการเคลือบผิวของงานชุบสังกะสีด้วยไฟฟ้า

สาขาวิชา วิทยาศาสตร์นาโนและเทคโนโลยี

ปีการศึกษา 2559

ลายมือชื่อนิติกร

ลายมือชื่อ อ.ที่ปรึกษาหลัก

ลายมือชื่อ อ.ที่ปรึกษาร่วม

5587854920 : MAJOR NANOSCIENCE AND TECHNOLOGY

KEYWORDS: ZINC; PASSIVATION; ELECTRODEPOSITION; MICRO/NANOSTRUCTURE; CORROSION

NARIN JANTAPING: NANOSTRUCTURAL INVESTIGATION AND ENGINEERING OF ELECTRODEPOSITED ZINC COATINGS AND THEIR CHROMIUM AND GRAPHENE-BASED PASSIVATION LAYERS. ADVISOR: ASSOC. PROF. DR. YUTTANANT BOONYONGMANEERAT, CO-ADVISOR: PROF. DR. CHRISTOPHER A.SCHUH, pp.

Electrodeposited zinc is an important type of coating used widely for corrosion protection in various applications. Nevertheless, the understanding on the relationships between coating fabrication process, micro/nanostructure, and properties of the material is rather limited. This thesis aims to develop structure-corrosion property relationship frameworks for the electrodeposited zinc coating and its chromium conversion layer, and also explore the novel process, particularly top-coating of graphene, upon which the corrosion resistance of the zinc coating could be enhanced. The research works performed in this thesis are divided into 3 parts: (i) the processing-structure-property relationships in electrodeposited zinc, (ii) the effects of the EZ's structure on the formation of Cr(III) passivation, and (iii) the feasibility of graphene-based coatings as a potential for protecting corrosion.

A set of environmentally friendly alkaline non-cyanide zinc coatings with and without trivalent chromium passivation is prepared by the electrodeposition process for examination of their micro/nanostructure and corrosion properties. Three groups of plating additives are employed to modulate the structure of the galvanized coating. Using a suite of modern characterization techniques, including field emission scanning electron microscopy (FE-SEM), X-ray diffractometry (XRD), focused ion beam (FIB), and transmission electron microscopy (TEM), it is determined that texture and interfacial defects which are controlled by additive incorporation play critical role in controlling the corrosion behavior of the coatings. Furthermore, polyquaternary amine salt is identified as an effective additive for zinc plating as it helps promotes a formation of a relatively thick amorphous-oxide phase in the chromate film resulting in high resistance to corrosion. Finally, the feasibility study of graphene-based top coatings for corrosion shows that graphene can be coated onto a substrate using the electroplating setup. The coating of graphene is found to be controlled by additives, applied current density, and deposition time. The resulting graphene coating shows appreciable corrosion resistance results, and thus it is promising to be used for top-coating of electrogalvanized zinc.

Field of Study: Nanoscience and Technology

Academic Year: 2016

Student's Signature

Advisor's Signature

Co-Advisor's Signature

ACKNOWLEDGEMENTS

I gratefully acknowledge the Thailand Research Fund through the Royal Golden Jubilee Ph.D. Program (PHD/0086/2554) for financial support, and the grant for the Surface Coatings Technology for Metals and Materials Research Unit (GRU 57-005-62-001), the grant for International Research Integration: Chula Research Scholar (GCRS_58_02_21_01), Ratchadaphiseksomphot Endowment Fund.

I would like to express my gratitude to my advisor, Assoc. Prof. Dr. Yuttanant Boonyongmaneerat, Deputy Director of Metallurgy and Materials Science Research Institute (MMRI), Chulalongkorn University, Thailand for big help and support in all of Ph.D. student's life. I am appreciated for his teaching, training, and inspiring.

My gratitude is also extended to my co-advisor, Prof. Dr. Christopher A. Schuh, Head Department, Department of Materials Science and Engineering, Massachusetts Institute of Technology (MIT), USA for support on aboard research and thesis guidance.

I would like to thank Dr. Shiahn Chen, collaborator, Research Specialist at the MRSEC Shared Experimental Facilities at MIT for teaching and supporting the focused ion beam (FIB) technique.

I am thankful to all thesis committees, including, Assoc. Prof. Dr. Vudhichai Parasuk, Assoc. Prof. Dr. Yuttanant Boonyongmaneerat, Prof. Dr. Christopher A. Schuh, Dr. Ratthapol Rangkupan, Dr. Nadnudda Rodthongkum, Dr. Wannipha Amatyakul for suggestions and guidance in thesis.

I would like to specially thank to Okuno-Auromex (Thailand) Co., Ltd. for support the research facility on chemical substance and analytical instruments.

I am thankful to the Program in Nanoscience and Technology (Interdisciplinary Program), Graduate school, Chulalongkorn University for the Ph.D. education.

I would like to thank the Metallurgy and Materials Science Institute (MMRI) and for support the research facility and the guidance in the thesis.

I would like to specially thank PORETEGE RESEARCH GROUP for friendship, teamwork, and researching facility.

I am thankful to the National Metal and Materials Technology Center (MTEC) for support the characterization techniques.

Finally, I gratefully acknowledge my parent, my family, and my friend for all best support and inspiration.

CONTENTS

	Page
THAI ABSTRACT	iv
ENGLISH ABSTRACT.....	v
ACKNOWLEDGEMENTS	vi
CONTENTS.....	vii
LIST OF TABLES	1
LIST OF FIGURES	2
CHAPTER I INTRODUCTION.....	4
1.1 Overview.....	4
1.2 Motivation.....	6
1.3 Research objective	7
1.4 Scope of research	8
1.5 Benefits of research	9
CHAPTER II LITERATURE SURVEY	10
2.1 Electrodeposited zinc (EZ)	10
2.2 Chromate passivation layers	13
2.3 Graphene-based coatings	14
CHAPTER III EXPERIMENTAL PROCEDURE.....	17
Part I. The processing-structure-property relationships in electrodeposited zinc....	17
3.1.1 Sample fabrication.....	17
3.1.2 Sample preparation and characterization	18
3.1.2.1 Sample preparation for surface morphology analysis	18
3.1.2.2 Cross sectioning for metallography.....	18
3.1.2.3 Sample preparation for crystal structure analysis.....	19
3.1.2.4 Sample thinning for structural analysis	19
3.1.2.5 Sample preparation for corrosion analysis	19
Part II. The effects of the electrodeposited-zinc structure on the structure of chromium-trivalence passivation.....	20
3.2.1 Sample fabrication.....	20

	Page
3.2.2 Sample preparation and characterization	20
Part III. The feasibility of graphene as a potential for protecting corrosion.....	22
3.3.1 Sample fabrication.....	22
3.3.2 Sample preparation and characterization	23
3.3.2.1 Sample preparation for surface morphology analysis	23
3.3.2.2 Sample preparation for crystal structure analysis.....	24
3.3.2.3 Sample preparation for chemical structure analysis.....	24
3.3.2.4 Sample cross sectioning for thickness measurement	24
3.3.2.5 Sample preparation for corrosion analysis	24
3.4 Detailed characterization techniques	25
3.4.1 Morphology analysis	25
3.4.2 Crystal structure analysis.....	25
3.4.3 Structural analysis via FIB and TEM	26
3.4.4 Corrosion analysis	28
CHAPTER IV EXPERIMENTAL RESULTS AND DISCUSSION.....	30
Part I. The processing-structure-property relationships in electrodeposited zinc....	30
4.1.1 Surface morphology	30
4.1.2 Crystallite size	31
4.1.3 Crystallographic texture	32
4.1.4 Corrosion behavior of electrodeposited zinc.....	36
4.1.4.1 Potentiodynamic polarization scan.....	36
4.1.4.2 Salt spray test.....	37
4.1.5 Relationship between structure and corrosion behavior of EZ	39
Part II. The effects of the electrodeposited-zinc structure on the structure of chromium-trivalence passivation.....	43
4.2.1 Surface morphology	43
4.2.2 Through-thickness structure	44
4.2.3 Corrosion behavior of passivated electrodeposited zinc	46
4.2.3.1 Potentiodynamic polarization scan.....	46

	Page
4.2.3.2 Salt spray test.....	48
4.2.4 Relationship between structure and corrosion behavior of EZP	50
Part III. The feasibility of graphene as a potential for protecting corrosion.....	51
4.3.1 Surface morphology	51
4.3.2 Surface structure.....	53
4.3.3 Through-thickness structure	54
4.3.4 Corrosion behavior of graphene-based coatings	56
4.3.4.1 Potentiodynamic polarization scan.....	56
4.3.4.2 The accelerated corrosion test	57
CHAPTER VI CONCLUSION	59
Part I. The processing-structure-property relationships in electrodeposited zinc.....	59
Part II. The effects of the electrodeposited-zinc structure on the structure of chromium-trivalence passivation.....	60
Part III. The feasibility of graphene as a potential for protecting corrosion.....	60
.....	62
REFERENCES	62
APPENDIX.....	71
OUTPUT.....	77
VITA.....	79

LIST OF TABLES

Table 1 Sample preparation details of the specimens in the current study.	21
Table 2 Corrosion properties (corrosion current density (I_{corr}), corrosion rate (CR), and percent red rust (RR)) of the specimens from different groups, as assessed by the potentiodynamic polarization and salt spray tests.	39



LIST OF FIGURES

Figure 1 The flowchart of the methodology of electrogalvanized and chromium coatings.	21
Figure 2 The synthesis of electrolyte and the plating condition of graphene-based coatings.	23
Figure 3 Micrographs showing the steps of TEM sample preparation via FIB techniques: (a) an electrogalvanized specimen is milled in cross-section by FIB; (b) a 1 μm thin lamellae was prepared using the H-bar FIB technique; (c) the manipulator probe lifted-out the lamellae and transfer it to a TEM grid; (d) FIB milling was further performed to thin the lamellae to about 50 nm.	27
Figure 4 Tafel plot and their extrapolated cathodic and anodic current for corrosion current and potential determination.	29
Figure 5 FE-SEM micrographs showing surface morphology of (a) EZ0, (b) EZ1, (c) EZ2, and (d) EZ3 samples.	31
Figure 6 The electrogalvanized specimens of different groups were analyzed with XRD to provide: (a) XRD profiles; (b) estimated crystallite size; and (c) texture coefficient.	34
Figure 7 TEM micrograph showing atomic arrays and grains of the electrogalvanized zinc sample from group EZ1.	34
Figure 8 Combined 3-D pole figures of the electrogalvanized samples: (a) EZ1 (b) EZ2, and (c) EZ3. The high and low intensities are represented by red and blue contours, respectively.....	35
Figure 9 Tafel plots of the electrogalvanized specimens EZ1, EZ2 and EZ3, as obtained from the potentiodynamic polarization measurements.	36
Figure 10 The appearance of the electrogalvanized test specimens, EZ1, EZ2, and EZ3, following the salt spray test at different periods.	38
Figure 11 TEM micrographs showing the Zn/Fe interface of the electrogalvanized specimens: EZ1 (a;b), EZ2 (c;d), and EZ3 (e;f). Regions in the brackets of the left-hand side figures are magnified on the rights.	42
Figure 12 FE-SEM micrographs showing surface morphology of (a) EZP1, (b) EZP2, and (c) EZP3 samples.	43

- Figure 13** Stitched TEM micrographs showing a cross section of the chromate conversion layer of the specimen from group EZP3. Amorphous, amorphous-oxide, and oxide layers are observed in the structure.45
- Figure 14** TEM micrographs showing cross sections of the chromate conversion layer of the specimens from groups (a) EZP1, (b) EZZ 2, and (c) EZP3.46
- Figure 15** Tafel plots of the chromated electrogalvanized specimens EZP1, EZP2 and EZP3, as obtained from the potentiodynamic polarization measurements.47
- Figure 16** The appearance of the chromated electrogalvanized test specimens, EZP1, EZP2, and EZP3, following the salt spray test at different periods.....49
- Figure 17** The surface morphology of the specimens. (a) and (b) are the micrograph of the steel substrate under the magnify of 200X and 2,000X, respectively. (c) and (d) are the micrograph of the graphene coatings under the magnify of 200X and 2,000X, respectively.52
- Figure 18** Chemical structure of the graphene-base coating, which was analyzed under X-ray photoelectron spectrometer (XPS). The binding energy of graphene structure is 285 eV at peak c1s1.53
- Figure 19** SEM micrographs showing surface morphology of the graphene-based coatings. The upper micrographs present the graphene coatings under current density of 2 A/dm² with increase the deposition time. The lower micrographs present the graphene coatings under current density of 1 A/dm² with increase the deposition time.....55
- Figure 20** SEM Micrographs showing the cross-section prepared by FIB technique. (a) is the the thickness of graphene-based coating. (b) is the high magnify micrograph which presents the thickness of graphene approximately 80 nm.56
- Figure 21** Tafel plots of the specimens, including graphene-based coating (G/STEEL), steel substrate (STEEL), electrodeposited zinc (EZ), graphene coated zinc (G/EZ), electrodeposited zinc with chromate passivation (EZP).....57
- Figure 22** The digital images of the specimens before and after 2-day immersion in 50 wt.% in NaCl: (a) and (b) are the steel substrate and (c) and (d) are the graphene-based coatings.58

CHAPTER I INTRODUCTION

1.1 Overview

The steel industries such as automotives, electronics and households, which utilize steels as a major component for their manufacturing, are constantly in need for developing the coating-materials and processings that effectively provide corrosion resistance for the steel structures [1-11]. Electrogalvanized coating, also known as electrodeposited zinc (EZ), which refers to an application of zinc coatings onto steel surfaces via the electrodeposition process, has been employed widely for corrosion protection [12-14]. In the process, electrodeposition represents the most advantages, including relatively high speed, high purity, and easy to adjust of composition and thickness [15, 16]. Nevertheless, thus far, a scientific understanding of the relationship between the microstructure and corrosion behaviors of electrodeposited zinc has not been fully established. This is at least partly an issue of scale and complexity: zinc coatings have intricate micro/nano-structural features, and are often capped with an extremely thin (and difficult to characterize) chromate conversion coating (CCC), which require a systematic and comprehensive study with an aid of advanced techniques for characterizations [17-19]. Among the relevant structural features, surface morphology [20, 21], crystallite size [22-24], and texture [25-30], have all been noted to influence corrosion behaviors of galvanized coatings. However, detailed analysis of crystallographic structure and nano-structure of

passivated electrogalvanized coatings and their influence on corrosion behaviors are yet to be carried out.

Even though EZ has been used extensively, the understanding on the relationship between structure and properties were limited. The challenges of these studies are divided into two parts (i) the effects of EZ's structure on the corrosion properties and chromium-trivalence Cr(III) passivation abilities, which were the decorative and anti-corrosive layers. Previously, the studies were obstructed by several problems. For examples, the thickness of the EZ is quite thin, approximately 5-25 micron [31]; the crystallite size is tiny in the scale of 20-90 nm [32, 33]; the surface is easy to oxidize at the normal atmosphere [34, 35]. Also, there were some problems in the study on Cr(III) passivation. For examples, the process is complexly; the thickness is in the order of a few nanometer approximately 100-500 nm [36]. (ii) The alternative materials for passivation. There have the needs of the new materials that presented the outstanding properties of corrosion resistance. However, there are the needs for more understandings on the process-structure-property relationships in the EZ.

One of the approaches involves introducing a novel type of materials that exhibits interesting properties to the coatings. Recently, graphene, an allotrope of carbon, is one-atom-thick planar sheets, which are densely packed in a honeycomb crystal lattice [37]. According to its properties: high strength (1TPa) and high corrosion resistance, it might be used for the surface coating materials to protect corrosion of the based metal [38-41].

The present study employs a suite of several complementary characterization techniques to systematically analyze the texture, microstructure, and nano-scale features of electrogalvanized coatings and their CCC and graphene-based passivation layers, in order to establish a structure-corrosion relationship framework for them. Three representative sets of alkaline non-cyanide based galvanized coatings produced under different conditions are studied, using field emission scanning electron microscopy (FE-SEM), X-ray diffractometry (XRD), focused ion beam (FIB), and transmission electron microscopy (TEM). The corrosion properties of the coatings are then evaluated in light of the microstructure analysis, and general principles for improved coating performance are identified. The understanding gained from this study should enable the development of enhanced corrosion resistant coatings via micro/nano-structural tailoring and engineering.

1.2 Motivation

The motivations of this research are divided into three parts below:

1. Although, it has several studies on the relationship between structure and corrosion properties of electrodeposited zinc (EZ). But it lacks of study on the processing-structure-property relationships in the EZ, with particular emphasis on the additive types to affect the crystal structure and corrosion resistance.

2. There have been studied on the appearances of chromium-trivalence (Cr(III)) passivation on the chemical compositions, structures and properties. But

there are fewer studies on the effects of the substrate's structure; typically the EZ, on the formation of Cr(III) passivation because the process is complexly and the thickness is in the order of a few nanometer approximately 100-500 nm. Therefore, the understanding gained from the first topic will lead to explain that the formation and the structure of Cr(III) passivation layer affected by the microstructure of the EZ.

3. The outstanding property of graphene is the strongest materials, which has the tensile modulus of 1 TPa. Moreover, it has the high corrosion resistant properties. In this case, it could be used for the surface coating materials to protect corrosion. Therefore, the development of graphene-based coatings might be used for protecting corrosion of the EZ.

1.3 Research objective

The objectives of this research are:

1. To study the processing-structure-property relationships in electrodeposited zinc produced from alkaline non-cyanide bath, with particular emphasis on the additive types to affect the crystal structure and corrosion resistance.
2. To investigate the effects of the electrodeposited-zinc structure on the structure of chromium-trivalence passivation layers.
3. To examine the feasibility of the plating conditions of graphene as a potential for protecting corrosion. There were two feasibility studies for graphene-based coatings: i) the feasibility of process for depositing graphene onto steel

substrate which were emphasized on the additive, current density, and deposited time.

ii) the feasibility of corrosion resistant property of the graphene-based coating.

1.4 Scope of research

The research focused on three topics:

1. The comparison of the effects of three types of additives, which have the different value of absorption strength, including, a mixture of imidazole and epihalohydrin (Lugalvan IZE), polyquaternary amine salt (Lugalvan P), and polyethyleneimine (Lugalvan G35) on the microstructure, crystal structure and corrosion properties of alkaline non-cyanide electrodeposited zinc.

2. The research concentrated on the effects of substrates EZ1, EZ2, and EZ3 on the microstructure, crystal structure, and corrosion responses of the chromium-trivalence passivation layers.

3. The research studied on the effects of the plating conditions which emphasis on the additive type, current density, and deposited time on the morphology, microstructure, crystal structure, and corrosion responses of the graphene-based coatings.

1.5 Benefits of research

The success of this research impacted to two sections. First, economics: the understanding gained from the research is critical for the development of the coatings that benefits the steel industry. Second, academics: a new knowledge of the surface coating technology that published in an international journal. The possibility of the topics for publication is listed below:

- The processing-structure-property relationships in electrodeposited zinc produced from alkaline non-cyanide bath, with particular emphasis on the additive types to affect the crystal structure and corrosion resistance.
- The effects of the electrodeposited-zinc structure on the formation of chromium-trivalence passivation.
- The feasibility of graphene-based coatings as a potential for protecting corrosion.

CHAPTER II LITERATURE SURVEY

2.1 Electrodeposited zinc (EZ)

Corrosion, a destruction of materials, is a process resulting from a chemical reaction between a metal and its environment [7]. It was also the most occurred problem in the steel industries such as automotives, electronics and households. According to its damages, the lost in the preventive and maintenance cost were expanded [42]. The world corrosion organization reported that the corrosion cost was up to \$U.S.2.2 trillion in 2012. In this reason, the research and development on the protection of corrosion have been needed to study profoundly and extremely [43].

There were several of surface-treatment techniques for protecting corrosion, including the cleaning for surface conversion, surface modification, coating, and so forth. Coating of metallic zinc was the economical techniques for protecting against corrosion [44]. Because it was higher corrosion resistance than iron and steel in the environment. Various methods of applying a zinc coating to iron and steel are in general uses: hot dip galvanizing, mechanical plating, spraying, and electroplating [44, 45]. Among the coating processes, electrodeposition represents the most advantages including relatively high speed, high purity, easy control of coating composition and thickness, and so on [15, 16].

In the process, zinc plating is a process of electrical and chemical reaction, which reduces zinc ions in electrolytes to form a zinc coating on electrode-steel-substrate [46, 47]. It was controlled by several important parameters [48]. For example, bath composition, which was including acid, alkaline cyanide, and alkaline non-cyanide. Among these baths, alkaline non cyanide was the most popular one in case of high throwing power and environmental friendly [15]. Moreover, enhancing the plating efficiency and producing the good appearances, additive agent has been used in the process. In order to the duties, it is the leveling agent, ion discharge stabilizer and brightener [49, 50]. There are two groups of additives [51]: inorganic and organic [52-55]. Among these additives, organic compound of polyamines were the most popular one that used for EZ, according to the wide length of ion discharge values. For example, Hsieh et al. studied on three types of polyamines, which including polyethyleneimine (Lugalvan G35), a mixture of imidazole and epihalohydrin (Lugalvan IZE) and polyquaternary amine salt (Lugalvan P) [56]. The results presented that all additives affect the adsorption strength or ion discharge in the difference value, but it was significantly improving the morphology. Additives were not only affecting the surface morphology and appearance of the EZ, but also influencing the crystal structure including microstructures and the crystal orientation or crystallographic textures.

It has been noted that crystal structure of EZ affects their corrosion properties [57-60]. Khorsand et al. [61], Park et al. [25], and Girin et al. [62] studied structural features that affect corrosion resistance of electrogalvanized coatings, and found that grain dissolution rate depends on which crystallographic planes are exposed. Ramanauskas et al. [30, 63] expanded the exploration of such crystallographic texture

effects in electrodeposited zinc and its alloys, and observed that packing density (and thus bond energy per unit area) of the exposed crystallographic planes is an important factor controlling their corrosion resistance. Furthermore, lattice imperfections and texture have been found to affect the properties of passivating oxide films and hence the coatings' corrosion resistance. Mouanga et al. [64] examined the influence of plating additives for zinc produced from chloride baths, and observed that the additives affect the texture and corrosion resistance of the deposits.

Together, the above studies have firmly established the importance of crystallographic texture on corrosion, and established that additives affect that texture as well as the structure of subsequent passivation layers for electrogalvanized coatings. Nevertheless, these data points are isolated and not well connected to one another, so the relationship between the plating additive usage, crystallographic orientations, and corrosion behavior must be inferred across studies, and is thus quite incomplete. Furthermore, preferred textures for electrogalvanized zinc that provide high resistance to corrosion remain inconclusive: Park et al. [25] and Ramanauskas et al. [30, 63] identify basal plane {001} surface normals as being preferred, whereas Girin et al. [62] and Mouanga et al. [64] suggested instead prismatic planes are preferred {110}. Finally, other microstructural factors affecting corrosion resistance including particularly the interface quality, do not appear to have been explored in detail.

2.2 Chromate passivation layers

Passivation layer is the topcoat layer of the electrodeposited samples, typically EZ, for the decorations [65, 66]. Chromium trivalence (Cr(III)), the environmentally friendly material, was the most popular passivation material for coating onto EZ [67-69]. It presented a good appearance with several colors via controlling the thicknesses, for example; thin film (< 80 nm) presented bright color, but thick film presented yellow, blue, and iridescent, respectively [37, 66]. Some metals added into the chromium solution to improve the color, for example, cobalt (Co) presents the dark black [70]. Recently, it has been reported that the chromium passivation layers presented the good property of corrosion resistance [71-73]. According to the outstanding properties of Cr(III) passivation, the processing is a key for controlling these properties.

Passivation processing is based on the electroless coatings, which is the chemical reaction of the coating materials to form layers onto the substrate without the electricity induction [74]. The formation of Cr(III) passivation was influenced by several parameters such as chemical concentration, temperature, time duration, and pH. There have been studied on the effects of parameters to the formation of the layer [75-79]. For example, On the hand Gigandet et al. [23], Fra, ckowiak et al. [24], and Long et al. [25] studied the structure of CCC with scanning electron microscopy (SEM), glow discharge spectroscopy, and x-ray fluorescence spectroscopy. They reported a variety of structures, including an amorphous oxide, a so-called “gel type” structure involving an amorphous matrix with small crystallites in it, and oxide layers

with compositions including Cr_2O_3 , $\text{Cr}(\text{OH})_3$, $\text{Cr}(\text{OH})\text{CrO}_4$, and $\text{Zn}_2(\text{OH})_2\text{CrO}_4$. The corrosion behaviors of Cr^{3+} and Cr^{6+} based CCC have been comparatively studied by Di Sarli et al. [26], Tomachuk et al. [27], and Rosalbino et al. [28]. Overall, these are far from complete studies. Particularly, the detailed microstructure of the CCC layer has yet to be revealed, and in the industrially relevant case of CCC-passivated Zn we are not aware of comprehensive work on structure-property relationships for corrosion coatings

Despite there have been studied the appearances and corrosion properties of Cr(III) passivation on the effects of these parameters [80-84], there were the needs for the further improvement and a better understanding of the EZ's structure on the formation of Cr(III) passivation layers.

2.3 Graphene-based coatings

One of the approaches involves introducing a novel type of materials that exhibits interesting properties to the coatings. Recently, graphene, an allotrope of carbon, is one-atom-thick planar sheets, which are densely packed in a honeycomb crystal lattice [37]. According to its properties: high strength (1TPa) and high corrosion resistance, it might be used for the surface coating materials to protect corrosion of the based metal [38-41].

There have been studies on graphene as the surface coating materials to protect corrosion of based metal [41, 85-88]. Various techniques used for coating graphene on to the based-metal. Among those, there are two popular techniques, which are the chemical vapor deposition (CVD) and the electrodeposition [89, 90]. The previous researches have looked at this subject argued against the techniques to synthesize graphene coatings via CVD and electrodeposition for corrosion resistant property. Shanshan Chen et al. [91], Kirkland et al. [86], and Dhiraj Prasai et al. [85], argued that the CVD was the technique that provides a single layer of high purity graphene. It was presented the small area in corrosion resistant. On the other hand, Hilder et al. [92] argued that the electrodeposition was the technique for coating graphene as a simple operation, low cost, and large area coating. The result showed that high efficiency of corrosion resistant was presented in the large area of coatings. Debate center on the issue was the efficiency of graphene coatings. As for, the techniques of coating via electrodeposition and CVD for corrosion resistant. The CVD technique was suitable for the high purity graphene coating with the small area, but the electrodeposition technique was suitable for the large area of graphene plating [89, 90, 93].

Electrophoretic deposition, a sub-process of electrodeposition, is the most process for deposit charged powder particles [94]. Graphene nanoplatelets had been also deposited via electrophoretic process. Graphene nanoplatelets were induced to form the charged graphene by additives (conductive polymer). There have been studies on graphene deposition via electrophoretic process [95, 96]. However, the high efficiency of graphene for protecting corrosion in the large scale were interested. Therefore, the condition for synthesizing and plating graphene coatings is very

important. Moreover, the understanding of these conditions will lead to achieve the coatings that protect corrosion in the other substrates, such as, steel or the electrodeposited zinc (EZ).



CHAPTER III EXPERIMENTAL PROCEDURE

This research studied on three topics including (i) the processing-structure-property relationships in EZ, (ii) the effects of the EZ's structure in the formation of Cr(III) passivation, and (iii) the feasibility of the plating conditions of graphene as a potential for protecting corrosion. Therefore, the methodology of this research is divided into three parts below:

Part I. The processing-structure-property relationships in electrodeposited zinc

3.1.1 Sample fabrication

Three sets of electrodeposited zinc samples were prepared from alkaline non-cyanide zinc electrolytes, having different types of organic additives, namely (i) a mixture of imidazole and epihalohydrin (Lugalvan IZE, BASF, Germany), (ii) polyquaternary amine salt (Lugalvan P, BASF, Germany), and (iii) polyethyleneimine (Lugalvan G35, BASF, Germany). These additives were selected in this study because they are the common levelers and brightening agents that are widely used commercially in environmentally-friendly electrogalvanizing systems [22-25], and are also known to provide electrodeposited zinc with distinct corrosion behavior [17, 18]. The electrolytes were prepared from a mixture of 10 g/l zincate ($\text{Na}_2\text{Zn}(\text{OH})_4$), 120 g/l sodium hydroxide (NaOH), and 1 ml/l of additive. For comparison, an additional set of electrogalvanized samples was prepared without using an additive.

Low carbon steel (5 x 7 x 0.1 cm) was used as substrate, countered by platinum mesh anodes for deposition. Prior to plating, the samples were soak-cleaned in a 50°C 50% NaOH solution for 30 mins, electro-cleaned in 5% NaOH (5V) for another 10 s, and finally dipped in 5% HCl for 10 s. Electrodeposition was carried out at room temperature using a current density of 0.02 A/cm² for 30 min, according to the optimal condition determined by Hull cell testing [97, 98]. Subsequently, the samples were cleaned, oven-dried, and kept in a desiccator.

3.1.2 Sample preparation and characterization

3.1.2.1 Sample preparation for surface morphology analysis

The sample was fitted onto the stage of FE-SEM (without conductive coating on the surface). Subsequently, the SEM micrographs were collected under the secondary electron mode.

3.1.2.2 Cross sectioning for metallography

Some basic challenges exist in its surface preparation process, which consists of (1) sample cutting, (2) mounting, (3) grinding, (4) polishing, and (5) etching. Due to the intrinsic sacrificial nature of electrogalvanized coating, the major issues being faced are developments of surface non-uniformity in the polishing step and localized corrosion attack induced by chemical etchants of the last step, which hinders visibility of the microstructural features. Whereas the first problem is commonly mitigated by using oil-based lubricants as polishing mediums, the best practice for the latter issue

remains unclear. Therefore, the present study has demonstrated the challenges and strategies of surface modification of electrogalvanized coatings for electron microscopy analysis [19]. For more information, a full paper is reported in *Appendix*.

3.1.2.3 Sample preparation for crystal structure analysis

Sample was cleaned and dried before testing. After that, sample was fit into the stage of XRD. Then, the leveling surface was adjusted. Finally, XRD was analyzed under the condition of two-theta scan.

3.1.2.4 Sample thinning for structural analysis

The most powerful technique for TEM sample preparation is focused ion beam (FIB), model Helios NanoLab™ 600i, 30kV. The sample was cut to form the size of 1 x 1 cm to fit into the FIB stage. After that, the sample was milling, and transferring to TEM grids. After the plated sample was welded on to the TEM grid, the thinning process was done until the thickness of 50 - 60 nm was achieved. Finally, TEM was employed for in-depth analysis of cross section microstructure details.

3.1.2.5 Sample preparation for corrosion analysis

The corrosion properties were studied by potentiodynamic technique and salt spray technique following ASTM B117 for surface- and interlayer corrosion behavior study, respectively. The solution of 5% NaCl was used in both techniques. The

sample for potentiodynamic was fit into the electrochemical cell with the analyzed area of 1 cm^2 . For the salt spray test, the sample was covered the edge with the protective tape for control the analyzed area for 5 cm^2 .

Part II. The effects of the electrodeposited-zinc structure on the structure of chromium-trivalence passivation

3.2.1 Sample fabrication

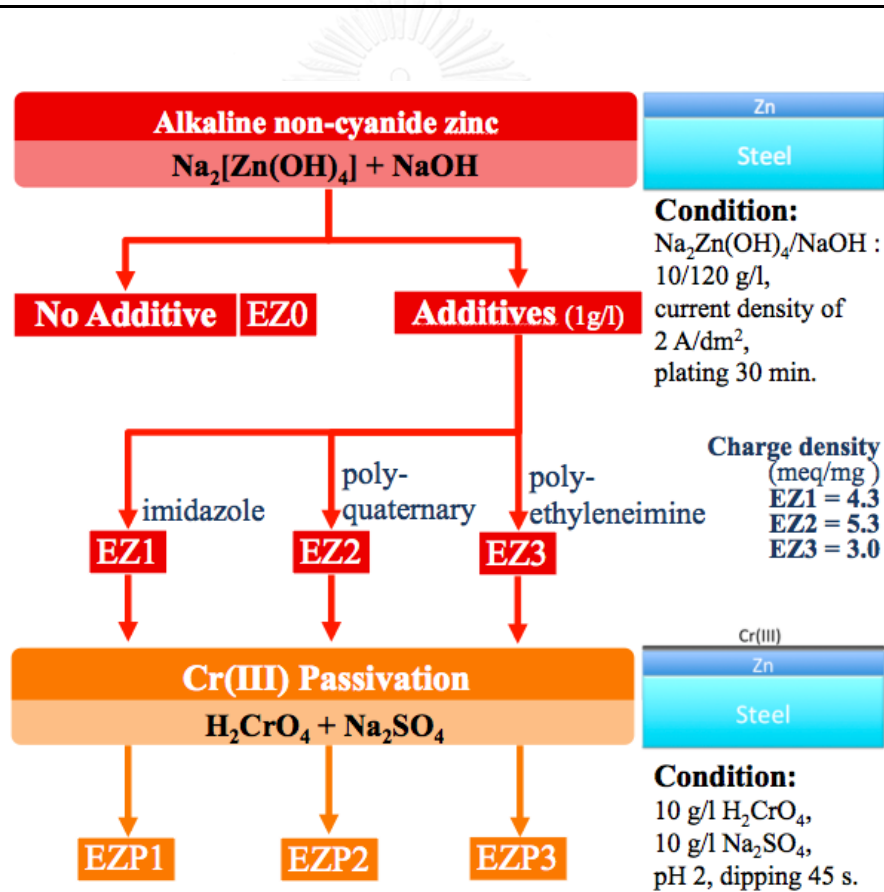
A set of the electrodeposited zinc samples from each group was further treated with chromate passivation, whereby the samples were dipped in a chromate conversion solution for a specified time, during which a CCC was developed on the galvanized surface [99-101]. The Cr(III) solution [102] employed herein was composed of 10 g/l of H_2CrO_4 and 10 g/l of Na_2SO_4 , with pH of 2. Each passivation treatment session was executed at 30°C for 45 s.

3.2.2 Sample preparation and characterization

Same as the part I (3.1.2)

Table 1 Sample preparation details of the specimens in the current study.

Sample name	Plating Additives	
As-galvanized	As-chromated	
EZ0	-	Without additive
EZ1	EZP1	A mixture of imidazole and epihalohydrin (Lugalvan IZE)
EZ2	EZP2	Polyquaternary amine salt (Lugalvan P)
EZ3	EZP3	Polyethyleneimine (Lugalvan G35)

**Figure 1** The flowchart of the methodology of electrogalvanized and chromium coatings.

Part III. The feasibility of graphene as a potential for protecting corrosion

3.3.1 Sample fabrication

The graphene electrolyte synthesized by using the graphene-nanoplatelets and additive. The specification of graphene nanopowder was the product No. 0541DX from Graphene Tech., USA. The average particle diameter was 15 micron and surface area 120-150 m²/g with the Carbon content of 99.5% purity. The 1 g/l of graphene nanoplatelet and 1 ml/l of additive were dispersed into the of 1 l. water. The selected additive for this study was the polyquaternary amine salt (Lugalvan P, BASF, Germany), which was the common levelers and brightening agents that was widely used commercially in environmentally-friendly electrogalvanizing system. In the synthesis of electrolyte process, diluted graphene nanopowder into electrolyte with additives and water. After that, disperse under 50 Hz for 10 hours.

After that, the samples from part I were used as a substrate for plating graphene electrolyte. The optimum current density and time duration determined by using Hull Cell test. The current densities for this study were 1 and 2 A/dm² and various deposition time from 0-30 min. Then all samples were baked, and kept into the desiccators to control the moisture. Finally, the characterization part was performed. Figure 1 shows the synthesis of electrolyte and the plating process of graphene-based coatings.

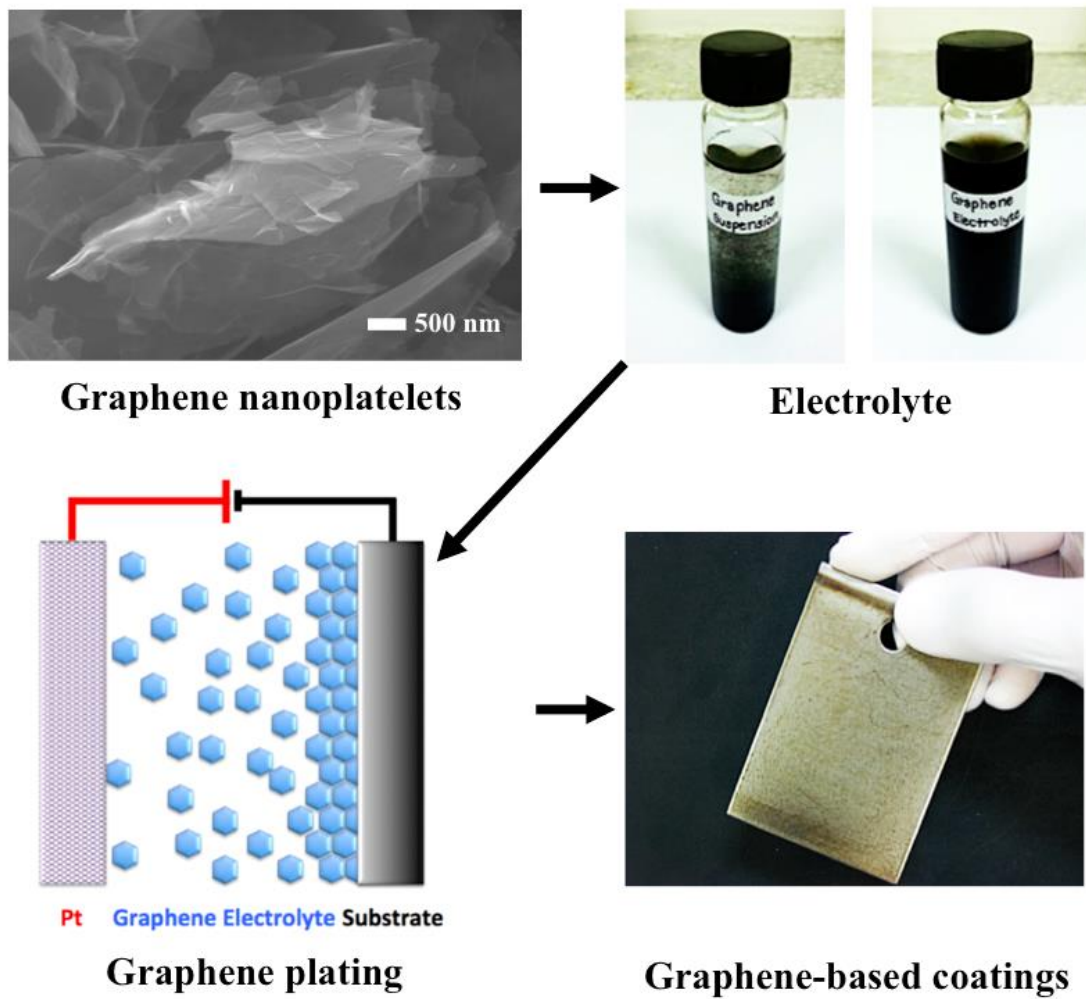


Figure 2 The synthesis of electrolyte and the plating condition of graphene-based coatings.

3.3.2 Sample preparation and characterization

3.3.2.1 Sample preparation for surface morphology analysis

Same as part I (3.1.2.1)

3.3.2.2 Sample preparation for crystal structure analysis

Same as part I (3.1.2.3)

3.3.2.3 Sample preparation for chemical structure analysis

X-ray photoelectron spectroscopy (XPS) is needed to analyze the graphene coating for confirming and understanding it. So, the sample was cut to form the size of 0.5 x 0.5 mm to fit into the sample holder for XPS analysis. After that, the sample was analyzed via XPS, AMICUS (Shimadzu), under a MgK α with 50 eV.

3.3.2.4 Sample cross sectioning for thickness measurement

The sample was cut to form the size of 1 x 1 cm to fit into the FIB stage. Before milling process, the Pt layer was coated for protecting the degradation of graphene layer during the milling process. After that, the sample was milled to observe to a thickness of graphene layer.

3.3.2.5 Sample preparation for corrosion analysis

The corrosion properties were studied by potentiodynamic technique and the accelerated corrosion test for surface- and interlayer corrosion behavior study, respectively. The solution of 5% NaCl was used in potentiodynamic technique. The sample for potentiodynamic was fit into analyzing cell with the analyzed area of 1 cm². The accelerated corrosion test, the sample was immersed into the 50% NaCl for 2 days.

3.4 Detailed characterization techniques

3.4.1 Morphology analysis

The surface morphology of the fabricated specimens was examined by field emission scanning electron microscopy, FE-SEM (Helios model Nanolab 600) operating at 5kV.

3.4.2 Crystal structure analysis

Crystal structure was analyzed by x-ray diffraction, XRD (RIGAKU, TTRAX III model) under 50kV and 300mA. The 2θ scan range was 30° – 80° with a step angle of 0.02° and scan speed of $5^\circ/\text{min}$. Scherrer's equation [103] was employed to estimate crystallite size (XS) from the instrumental broadening-corrected XRD profiles. The equation was presented below:

$$\text{Crystallite size} = \frac{k\lambda}{B \cos \Theta} \quad (1)$$

Where, λ is the wavelength of x-ray source. k is the unit cell geometry dependent constant that value is typically between 0.85 and 0.99. B is the peak broadening or the full-width-half-max (FWHM) of the each peak in the unit of radians. Bragg's angle (θ) is acquired from the plane $\{hkl\}$.

The texture coefficient (TC) of the planes preferentially oriented perpendicular to the surface normal direction was determined from the following equation [104]:

$$\text{Texture coefficient} = \frac{\frac{I_{hkl}}{I_{hkl}^0}}{\frac{1}{n} \sum \frac{I_{hkl}}{I_{hkl}^0}} \quad (2)$$

where, I_{hkl} and I_{hkl}^0 are the intensity of hkl reflections from zinc coatings and from a random sample (ICDD PDF No. 04-0831), respectively, and n is the number of selected planes. Additionally, the crystal orientations in 3-D, namely rolling (RD), transverse (TD), and normal (ND directions), were assessed through pole figures [105] with tilt angles (α) of 0°-90°, rotational angles (β) of 0°-360°, a 120°/min scan rate, and 5° interval step.

3.4.3 Structural analysis via FIB and TEM

In-depth analyses of the structure of the coatings and their interfaces were conducted using a transmission electron microscope, TEM (JEOL JEM-2010). For preparation of TEM specimens, a focused ion beam (FIB) milling system (Helios Nanolab 600) was employed for cross-sectional milling of the samples and transferring them to TEM grids where further ion thinning was conducted [106-108]. A series of images depicting the TEM sample preparation procedure is presented in Fig. 3.

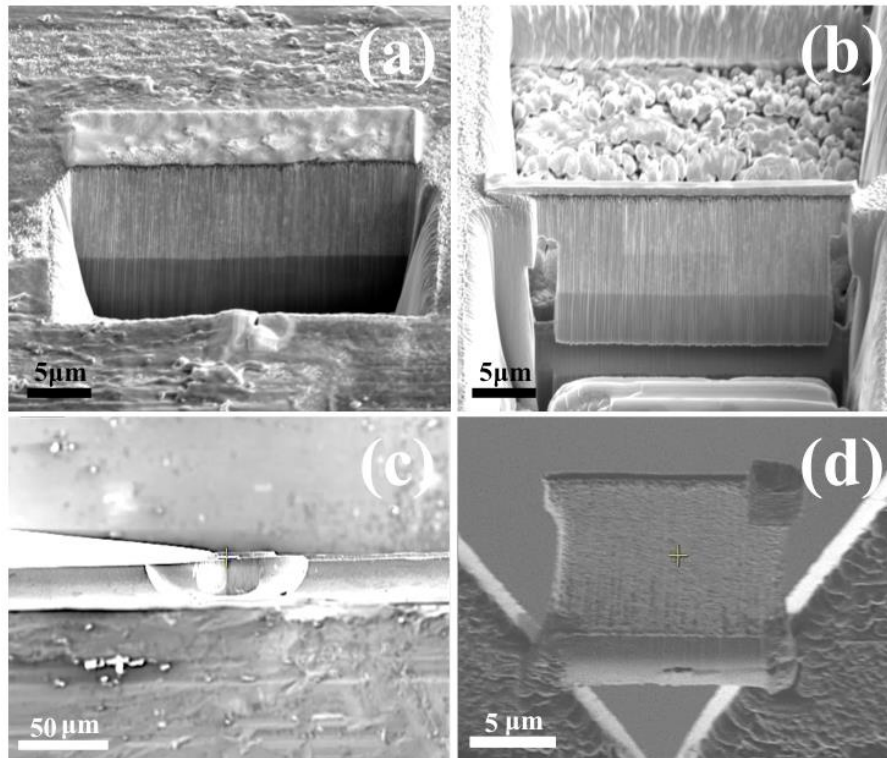


Figure 3 Micrographs showing the steps of TEM sample preparation via FIB techniques: (a) an electrogalvanized specimen is milled in cross-section by FIB; (b) a 1 μm thin lamellae was prepared using the H-bar FIB technique; (c) the manipulator probe lifted-out the lamellae and transfer it to a TEM grid; (d) FIB milling was further performed to thin the lamellae to about 50 nm.

3.4.4 Corrosion analysis

Two sets of tests were employed to characterize the corrosion properties of the coating materials. Firstly, salt spray tests (Q-Fog chamber, model CCT600), following ASTM B117, were performed to assess the corrosion behavior through the development of rust on the sample surface. The corroded area per total area, percent red rust (RR), were carried out by Imagej software. Secondly, using a potentiostat (μ Autolab type III), potentiodynamic polarization measurements were carried out to electrochemically quantify the corrosion rates of the samples. 5% NaCl solution was employed for both sets of tests.

Tafel plot is a tool for analyzing the corrosion behavior of the surface via Potentiodynamic polarization scan. Figure 4 shows the intersection between the extrapolated lines of anodic and cathodic is used for determining the corrosion current and potential. Moreover, the corrosion current is then calculated for the corrosion rate which expressed in unit of millimeters per year.

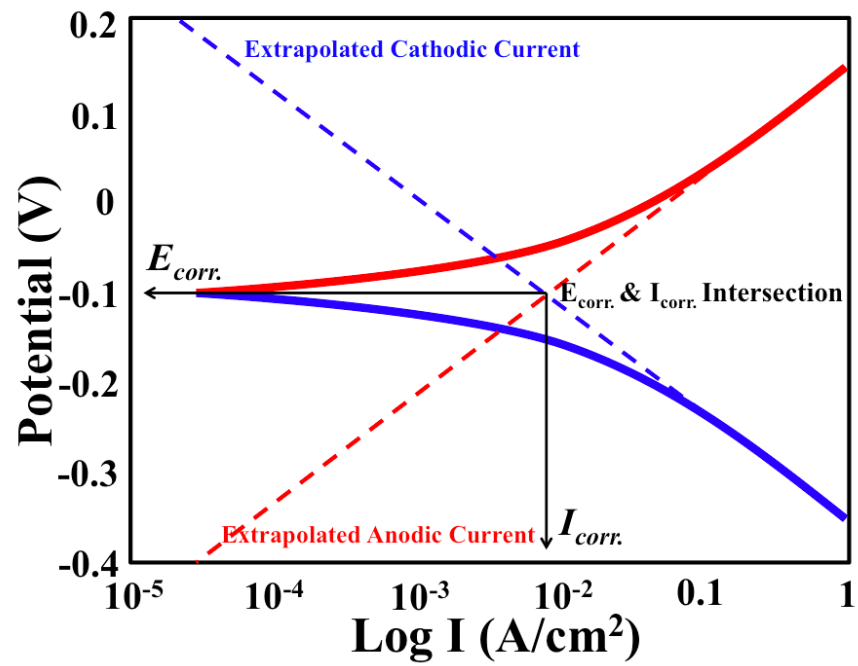
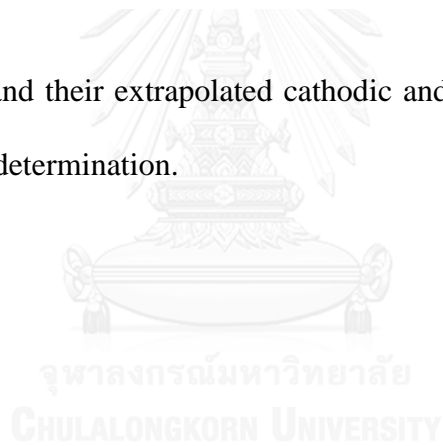


Figure 4 Tafel plot and their extrapolated cathodic and anodic current for corrosion current and potential determination.



CHAPTER IV EXPERIMENTAL RESULTS AND DISCUSSION

Part I. The processing-structure-property relationships in electrodeposited zinc

4.1.1 Surface morphology

The electrodeposited zinc coating samples of all groups, namely EZ0, EZ1, EZ2 and EZ3 all exhibited good uniformity. Micrographs showing the surface morphology of these specimens are presented in Fig. 5. Sample EZ0, with no use of plating additives (Fig. 5(a)), is characterized by coarse grains and a rather rough surface. On the other hand, those that use additives exhibit finer grains and low surface roughness. Furthermore, these deposits are relatively mechanically robust to handling as compared to EZ0. Upon a closer examination, EZ1, EZ2 and EZ3 show different surface morphologies (Fig. 5(b-d)), which are in line with their distinct textures to be discussed in the subsequent section.

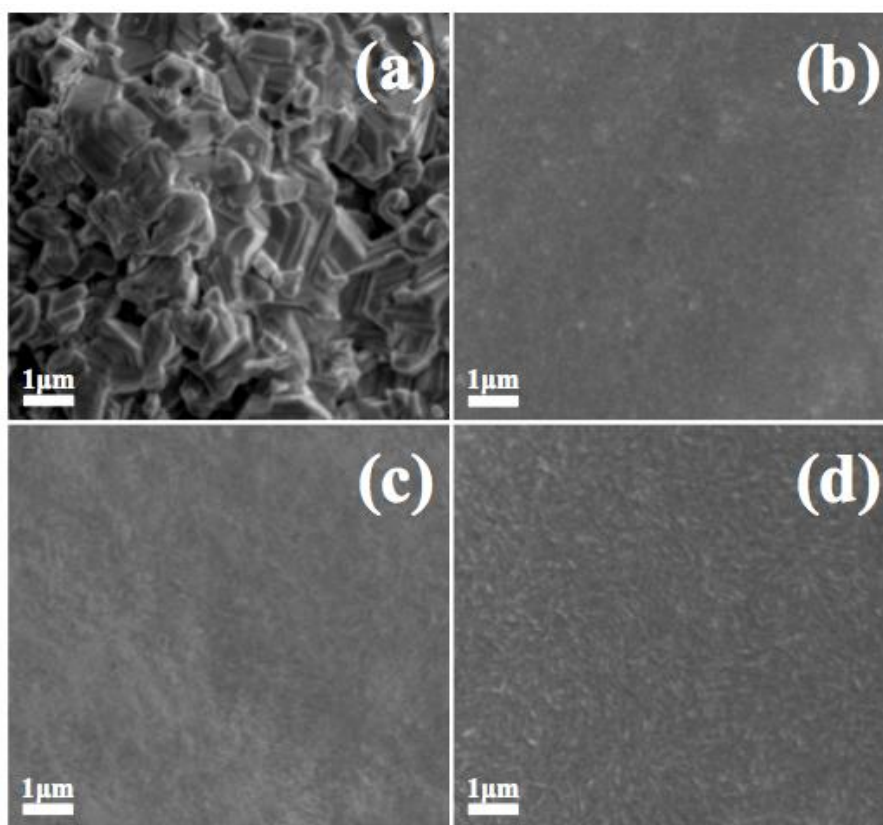


Figure 5 FE-SEM micrographs showing surface morphology of (a) EZ0, (b) EZ1, (c) EZ2, and (d) EZ3 samples.

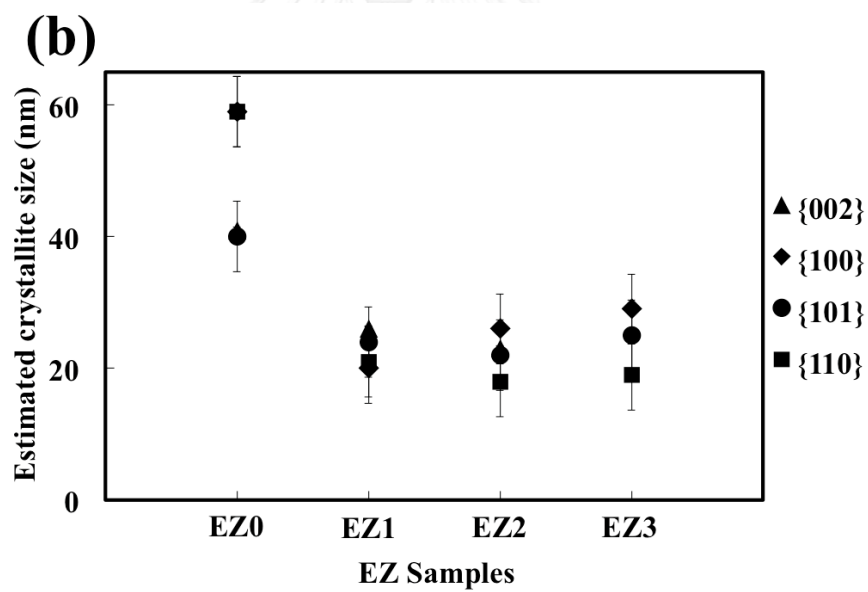
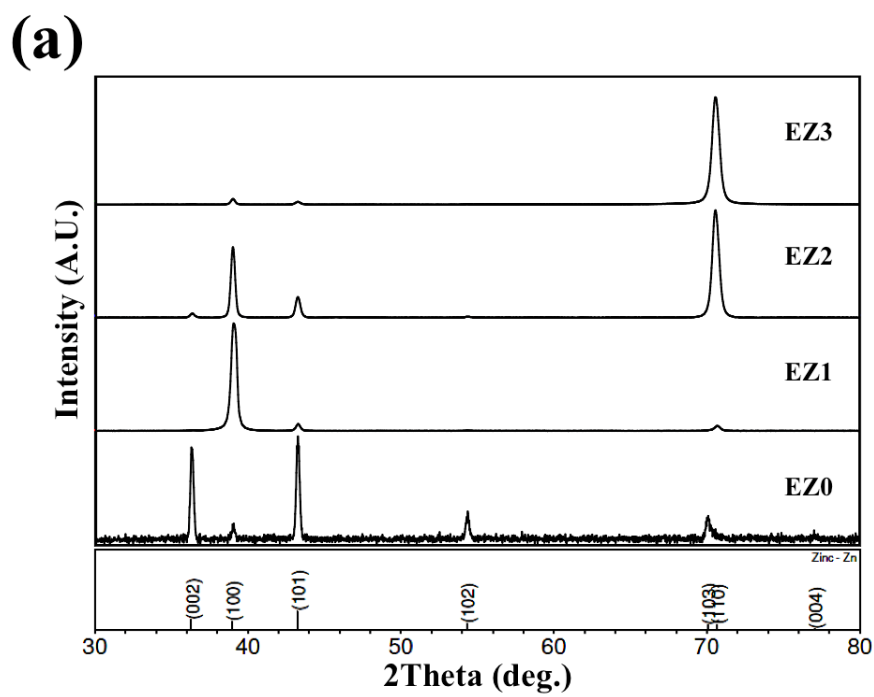
4.1.2 Crystallite size

The XRD profiles of the electrogalvanized samples of all groups presented in Fig. 6(a) confirm that all samples are comprised of a single phase of zinc, as expected. Using Scherrer's equation (Eq. 1), crystallite sizes of the deposits could be determined for the {002}, {100}, {101}, and {110} reflections as shown in Fig. 6(a). It can be observed that, overall, EZ0 exhibits relatively larger crystallite sizes, whereas the crystallite sizes of EZ1, EZ2, and EZ3 appear comparable at ~20 nm. Such small

crystallite sizes are underlined by bright-field TEM micrographs showing zinc grains and arrangements of zinc atoms, as exemplified by EZ1 in Fig. 7.

4.1.3 Crystallographic texture

Using the TC equation (Eq. 2) and relative XRD intensity of different crystal planes, the distribution of crystallographic orientations or texture of the polycrystalline deposits were determined. Fig. 6(c) shows the texture coefficients of {002}, {100}, {101}, and {110} planes of the specimens in all groups. EZ0 demonstrates preferred surface-normal orientations with {002} and {101} planes, whereas EZ1, EZ2, and EZ3 preferentially orient in the directions of {100} and {110} planes normal to the coating surface. Furthermore, the relative texture coefficients of different planes are somewhat distinct among EZ1, EZ2 and EZ3, as shown in Fig. 6(c).



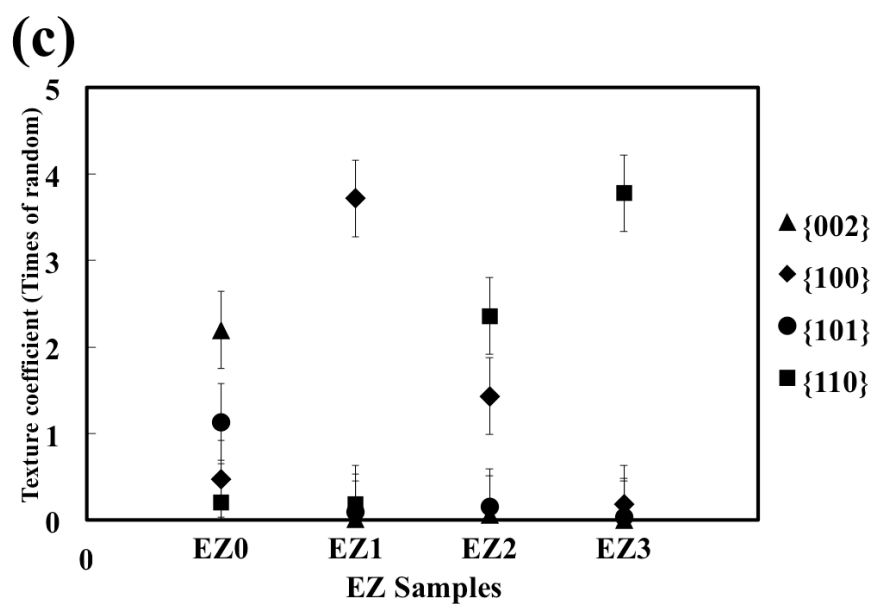


Figure 6 The electrogalvanized specimens of different groups were analyzed with XRD to provide: (a) XRD profiles; (b) estimated crystallite size; and (c) texture coefficient.

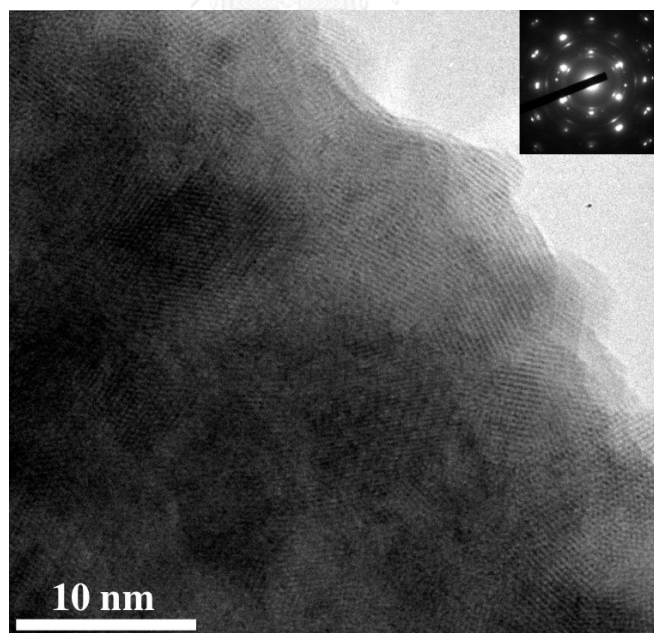


Figure 7 TEM micrograph showing atomic arrays and grains of the electrogalvanized zinc sample from group EZ1.

Figure 8 shows the combined results of the XRD pole figures obtained from the analysis of the four crystal planes of the specimens, namely $\{002\}$, $\{100\}$, $\{110\}$, and $\{101\}$. The results generally echo the 2D XRD profiles in Fig.6(a) and additionally indicate that the 3 groups of specimens (EZ1, EZ2, EZ3) all exhibit fiber textures. The pole figures demonstrate that the index planes, $\{100\}$, of EZ1, EZ2, and EZ3 respectively align normal to the surface, diffusively spread away from the surface normal, and concentrate at 60° of the tilt angle. The $\{100\}$ plane also corresponds to the lowest in-plane packing density, which has been suggested to correlate to corrosion resistance as described in the introduction; that the three specimens EZ1, EZ2, and EZ3 have different orientations of this plane is therefore convenient to explore a range of corrosion properties, as will be seen subsequently.

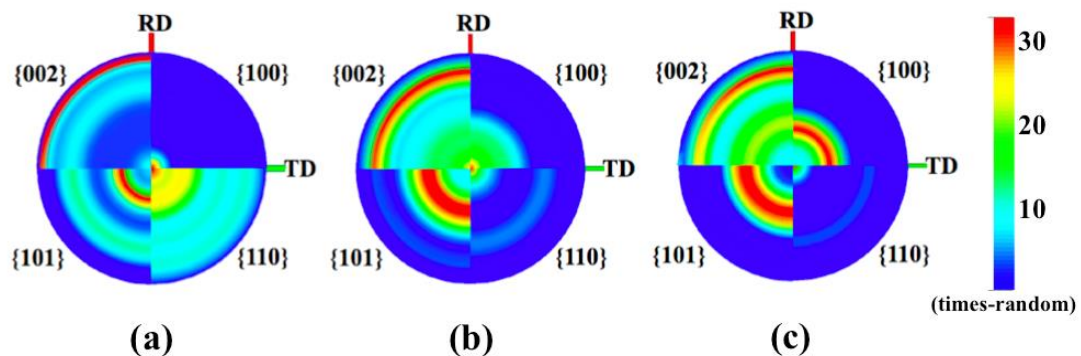


Figure 8 Combined 3-D pole figures of the electrogalvanized samples: (a) EZ1 (b) EZ2, and (c) EZ3. The high and low intensities are represented by red and blue contours, respectively.

4.1.4 Corrosion behavior of electrodeposited zinc

4.1.4.1 Potentiodynamic polarization scan

Figure 9 comparatively presents the potentiodynamic polarization results of the electrogalvanized samples in the EZ1, EZ2, and EZ3 groups, all of which exhibit a similar shape. Nevertheless, based on the values of the corrosion currents (I_{corr}), the corrosion rates (CR) of these samples vary somewhat, ranging from 0.424, 0.353, and 0.175 mm/year for EZ1, EZ2, and EZ3, respectively.

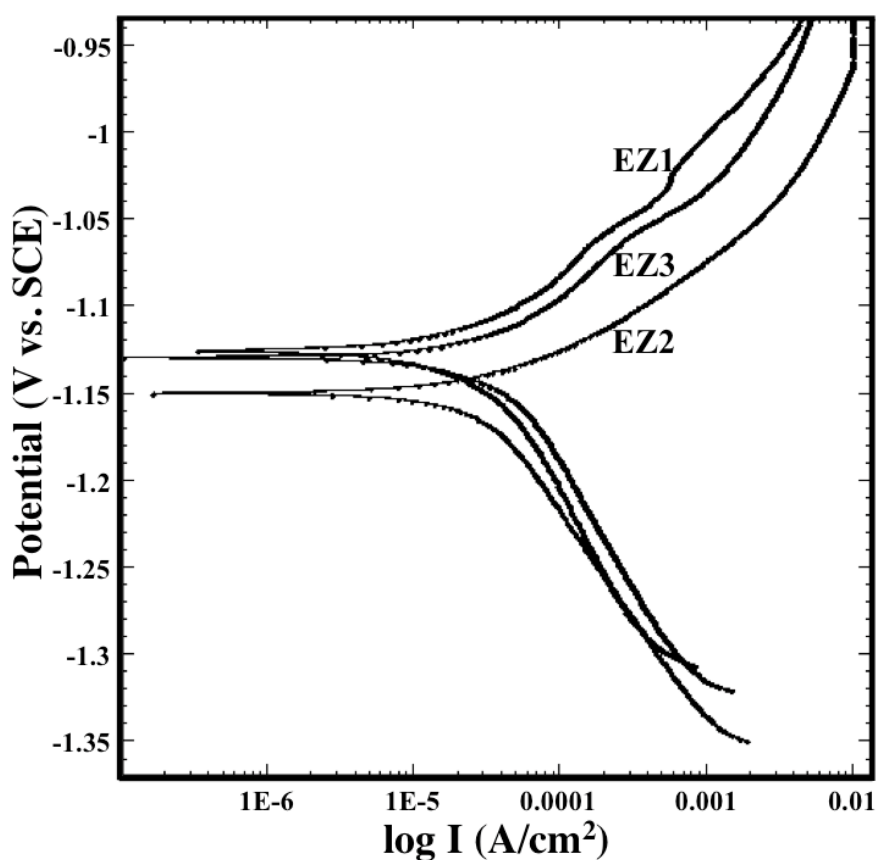
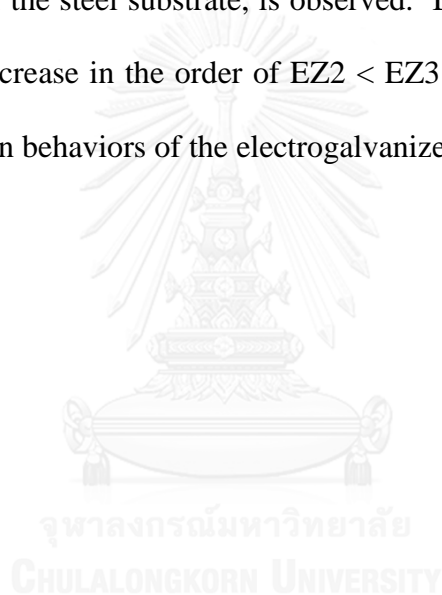


Figure 9 Tafel plots of the electrogalvanized specimens EZ1, EZ2 and EZ3, as obtained from the potentiodynamic polarization measurements.

4.1.4.2 Salt spray test

Figure 10 shows the surface appearance of the EZ samples at different stages of the salt spray test. As anticipated, white rust, which is comprised of the oxides and hydroxides of zinc [109], is initially formed across the samples' surface. Following the first 24 hrs, the content of the white rust of the different groups of samples appears to increase in the order EZ3 < EZ1 < EZ2. Later on, the development of red rust, owing to oxidation of the steel substrate, is observed. By the 360th hr, the amount of red rust appears to increase in the order of EZ2 < EZ3 < EZ1. Table 2 summarizes the results of corrosion behaviors of the electrogalvanized specimens.



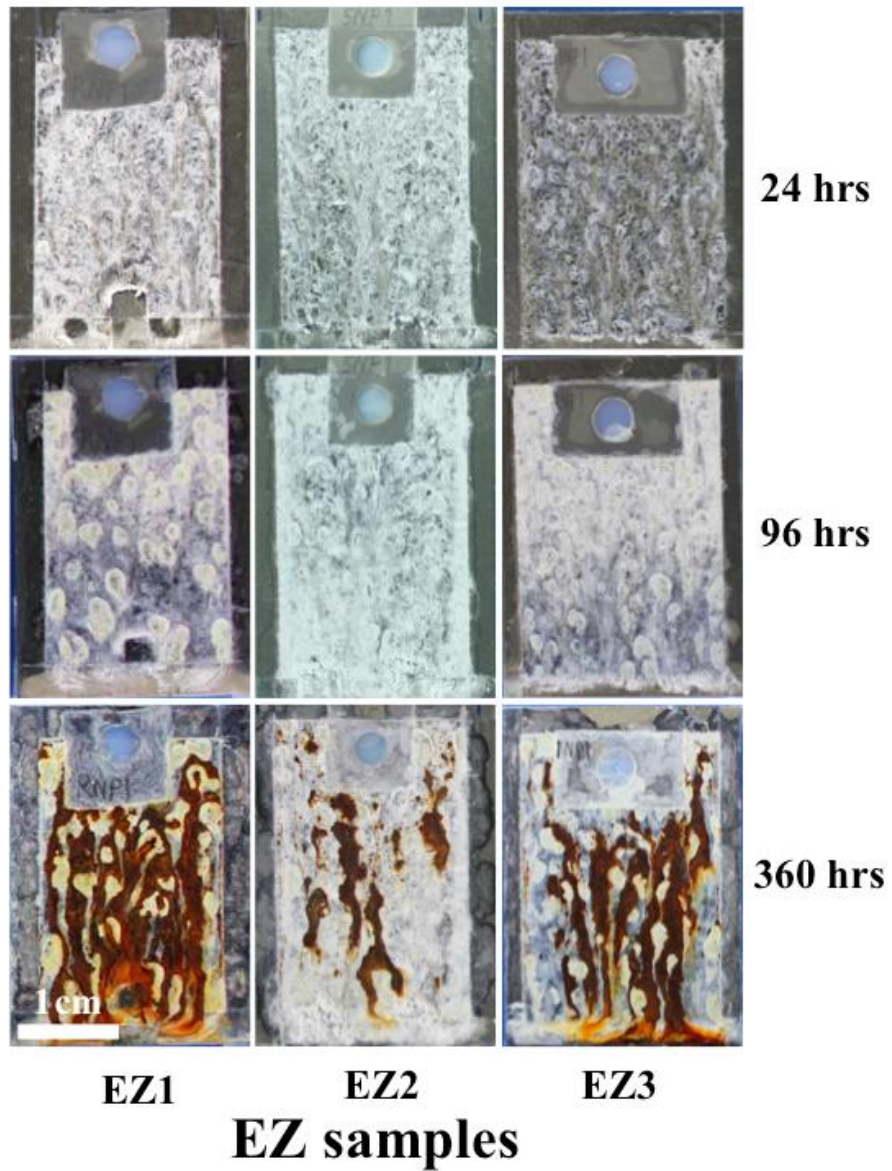


Figure 10 The appearance of the electrogalvanized test specimens, EZ1, EZ2, and EZ3, following the salt spray test at different periods.

Table 2 Corrosion properties (corrosion current density (I_{corr}), corrosion rate (CR), and percent red rust (RR)) of the specimens from different groups, as assessed by the potentiodynamic polarization and salt spray tests.

Sample name	Potentiodynamics		Salt spray	
	$I_{corr.}(\mu A)$	CR (mm/year)	RR (%)	
			360 hr	600 hr
EZ1	36.50	0.424	81	-
EZ2	30.35	0.353	28	-
EZ3	15.03	0.175	60	-
EZP1	1.16	0.014	-	10
EZP2	0.06	0.001	-	0
EZP3	0.95	0.011	-	0

4.1.5 Relationship between structure and corrosion behavior of EZ

Surface morphology and texture of the samples EZ0, EZ1, EZ2 and EZ3 are all distinct from one another, clearly the result of the plating additives, which serve as adsorbates, contributing to a reduction of the mean free path of the adions, and in effect influencing the nucleation, grain growth, and texture development [27, 110-112]. The three organic additives examined herein in fact have different levels of charge density (meq./mg), in an increasing order of polyquarternary amine salt (5.3) > imidazole and epihalohydrin (4.3) > polyethyleneimine (3.0) [35]. Their adsorption strength varies correspondingly, and these additives could in turn influence texture development of the deposits to different degrees.

Considering the corrosion resistance of the electrogalvanized specimens from the corrosion rates as analyzed by potentiodynamic polarization, the order of the samples with respect to increasing the resistance to corrosion is: $EZ1 < EZ2 < EZ3$. This result appears to be in line with the conventional understanding of how texture and crystallographic orientation can influence corrosion behavior – specifically, crystal planes with high packing density would exhibit relatively strong resistance to corrosion, and vice versa [29, 30, 113]. For hexagonal crystals, in particular, the order of crystal planes with respect to decreasing the atomic surface density is $\{002\} > \{110\} > \{101\} > \{100\}$. It thus has been generally found that zinc coatings with $\{002\}$ planes presented on the surface show relatively high surface hardness and high corrosion resistance [18, 19, 23]. Here, the weakly-packed atomic plane $\{100\}$ is increasingly dominant on the specimens' surface in the order of $EZ3 < EZ2 < EZ1$, which corresponds well to their increasing levels of the measured corrosion rates, respectively.

This reasoning connecting texture and corrosion, however, does not map well to the results obtained from the salt spray tests, which indicate that $EZ2$ exhibits highest resistance to red rust formation and corrosion among the three groups. In part, this is certainly because the salt spray environment is complex, dynamic, and not simply predicted by, e.g., a polarization analysis. To better understand the salt spray trends, TEM analysis was additionally conducted to examine the cross-section of the specimens. The resulting TEM bright field images presented in Fig. 11 reveal that specimens $EZ1$ and $EZ3$ exhibit voids and cracks close to the zinc/steel interface, whereas the interfacial microstructure of $EZ2$ is homogeneous and generally free of defects. Clearly, the presence of the interfacial defects in $EZ1$ and $EZ3$ could have

promoted corrosion and red rust formation, especially as the salt spray test proceeded, allowing saline electrolyte to progressively permeate along the channels of these defects and reach the steel substrates. The high level of charge density of polyquarternary amine salt in EZ2 could have promoted a relatively more stable electrodeposition session, leading to development of low residual stresses and hindrance of interfacial defect formation [114, 115].



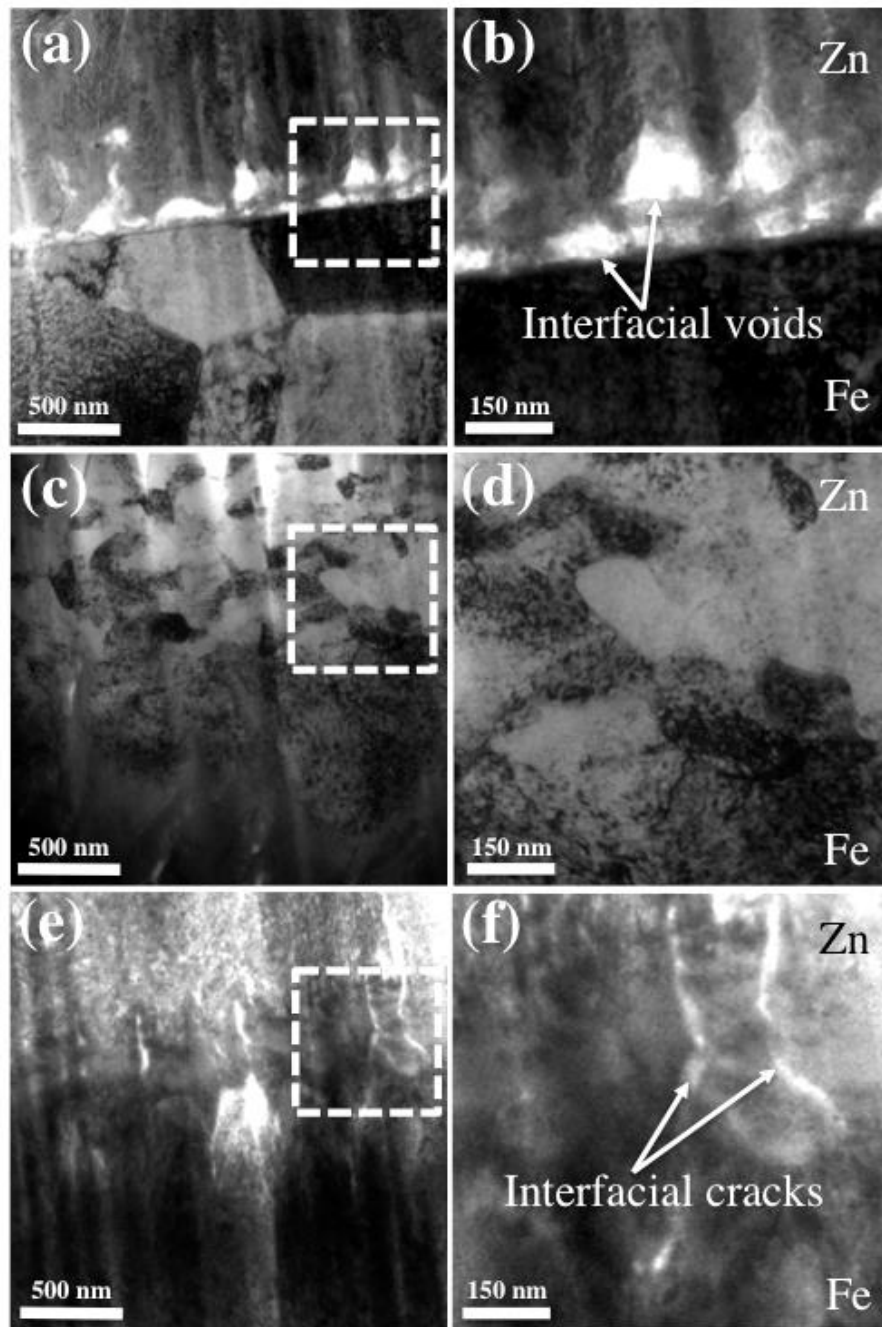


Figure 11 TEM micrographs showing the Zn/Fe interface of the electrogalvanized specimens: EZ1 (a;b), EZ2 (c;d), and EZ3 (e;f). Regions in the brackets of the left-hand side figures are magnified on the rights.

Part II. The effects of the electrodeposited-zinc structure on the structure of chromium-trivalence passivation

4.2.1 Surface morphology

Having a uniformly black-colored surface, all electrogalvanized samples appeared to be successfully treated with a chromate conversion process. Under a microscopic examination, it is observed that the surface of the passivated samples exhibits a mountain-range-like morphology, with short cracks distributed throughout the surface (Figs 12(a)-(c)).

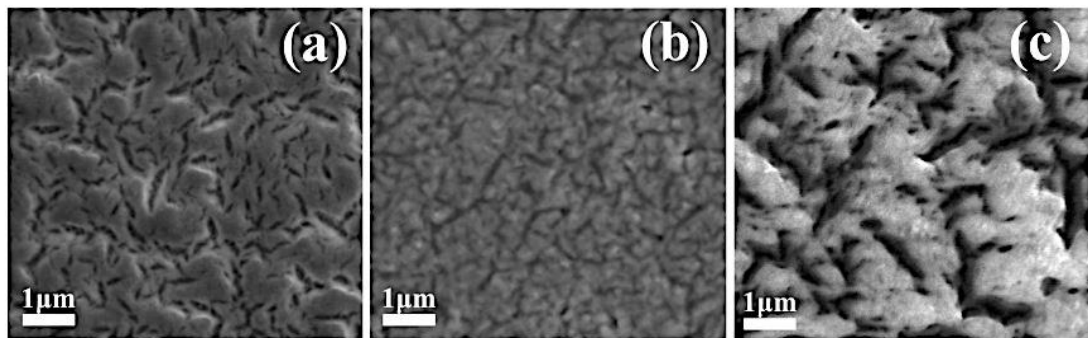


Figure 12 FE-SEM micrographs showing surface morphology of (a) EZP1, (b) EZP2, and (c) EZP3 samples.

4.2.2 Through-thickness structure

Using a combined technique of FIB and TEM, the through-thickness structure of the chromate conversion coating (CCC) specimens are analyzed, as exemplified by a representative TEM micrograph obtained from specimen EZP3 (Fig. 13). To the authors knowledge, this is one of the first TEM pictures that provide clear detail of the CCC structure. The crystallographic analysis indicates that the thin film composes of three sub-layers, listed from the outer surface to the substrate side: (i) amorphous, the metallic oxide complex, (ii) amorphous-oxide, trivalent chromium precipitates [23] comprising a mixture of amorphous matrix and crystalline phases, and (iii) crystalline oxides, the electrochemical combination between the metal and the metallic oxide. These structures are not aligned with those of prior studies, which proposed based on the glow discharge optical spectroscopy (GDOS) and X-ray photoelectron spectroscopy (XPS) that CCC films are composed of three layers of metallic oxide complex, trivalent chromium complex, and an oxide layer of $\text{Cr}(\text{OH})_3$, ZnO , and Cr_2O_3 , respectively [31-33].

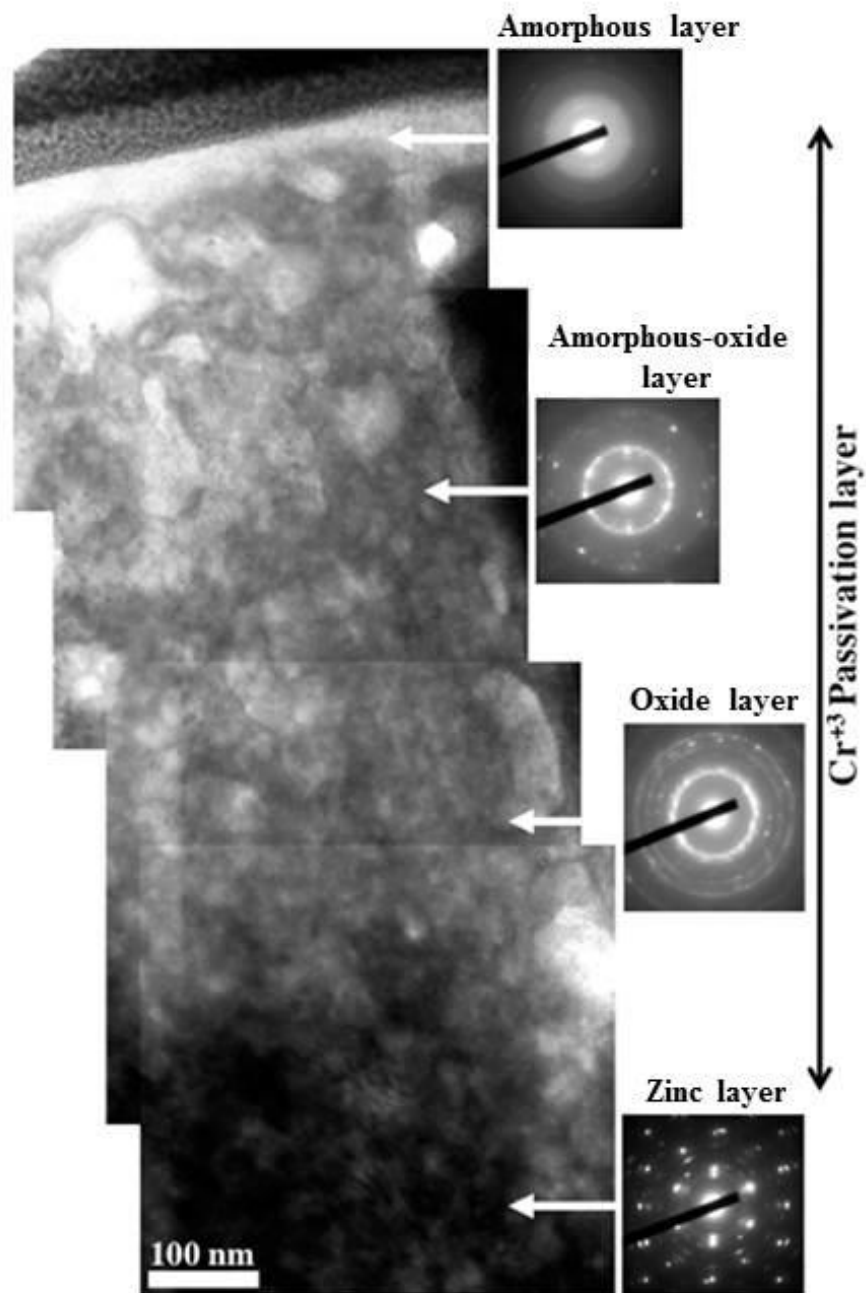


Figure 13 Stitched TEM micrographs showing a cross section of the chromate conversion layer of the specimen from group EZP3. Amorphous, amorphous-oxide, and oxide layers are observed in the structure.

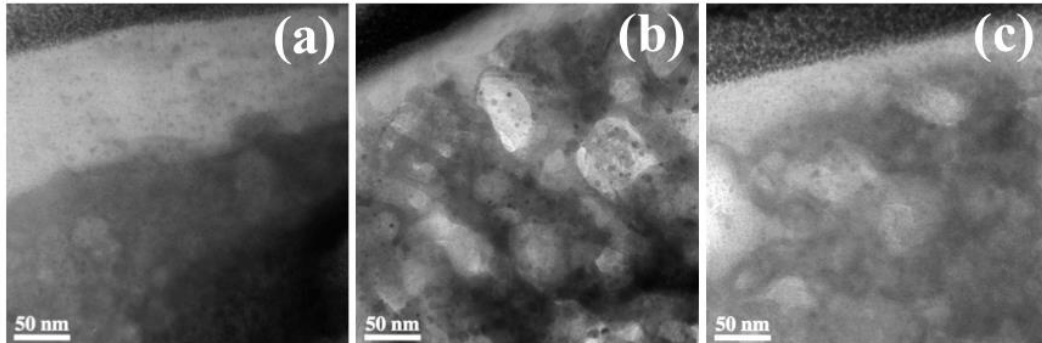


Figure 14 TEM micrographs showing cross sections of the chromate conversion layer of the specimens from groups (a) EYP1, (b) EYP 2, and (c) EYP3.

Comparing the through thickness structure of the CCC of the 3 specimens (EYP1, EYP2, EYP3) in Fig. 14, it is observed that the microstructure in EYP1 is somewhat distinct with that of EYP2 and EYP3 in that its amorphous layer is relatively thick and a grain structure in the amorphous-oxide layer is more refined. On the other hand, the microstructure of EYP2 and EYP3 is characterized by a thick amorphous-oxide layer, which contains grains of larger sizes.

4.2.3 Corrosion behavior of passivated electrodeposited zinc

4.2.3.1 Potentiodynamic polarization scan

Figure 15 comparatively presents the potentiodynamic polarization results of the electrogalvanized samples in the EYP1, EYP2, and EYP3 groups. These polarization curves exhibit rather distinct shapes, which is also reflected in large

variations of their corrosion currents (I_{corr}) and hence the corrosion rates (CR). CRs of the samples are found to increase in the order of $\text{EZP1} < \text{EZP3} < \text{EZP2}$.

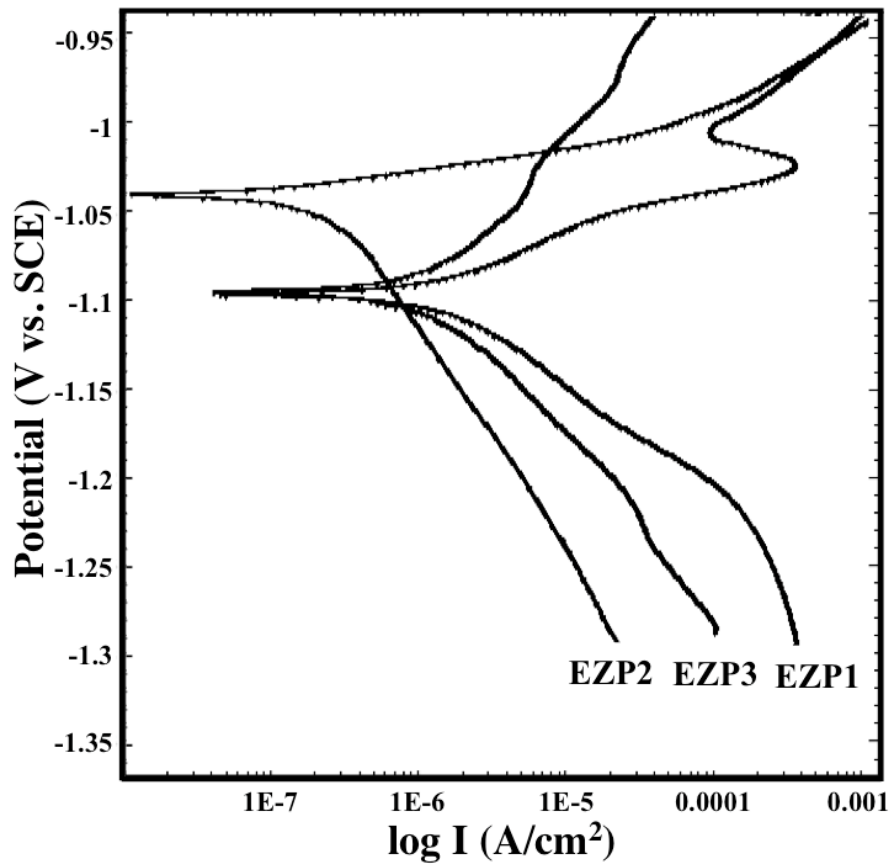
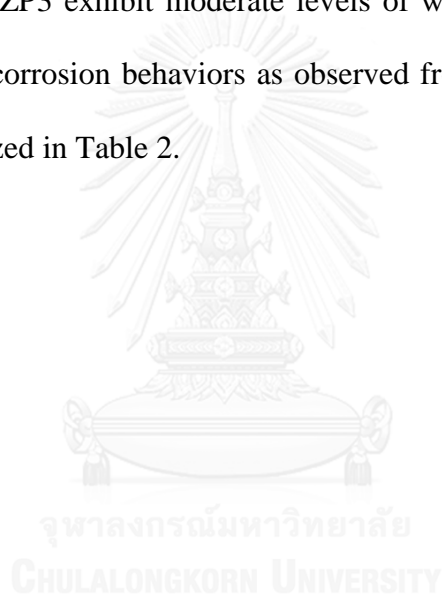


Figure 15 Tafel plots of the chromated electrogalvanized specimens EZP1, EZP2 and EZP3, as obtained from the potentiodynamic polarization measurements.

4.2.3.2 Salt spray test

Figure 16 shows the surface appearance of the EZP samples at different stages of the salt spray test. After 72 hours, white stains appear across the samples' surfaces, with EZP2 and EZP3 showing a relatively high amount of staining. As time proceeds, however, EZP1 develops white rust at a faster pace compared to others. The vivid white rust spots on EZP1 surface suggest that corrosion has reached the zinc layer of the sample. By the 600th hr, red rust and large white spots are observable on EZP1, whereas EZP2 and EZP3 exhibit moderate levels of white stain and are free of red rust. The results of corrosion behaviors as observed from the salt spray test of EZP samples are summarized in Table 2.



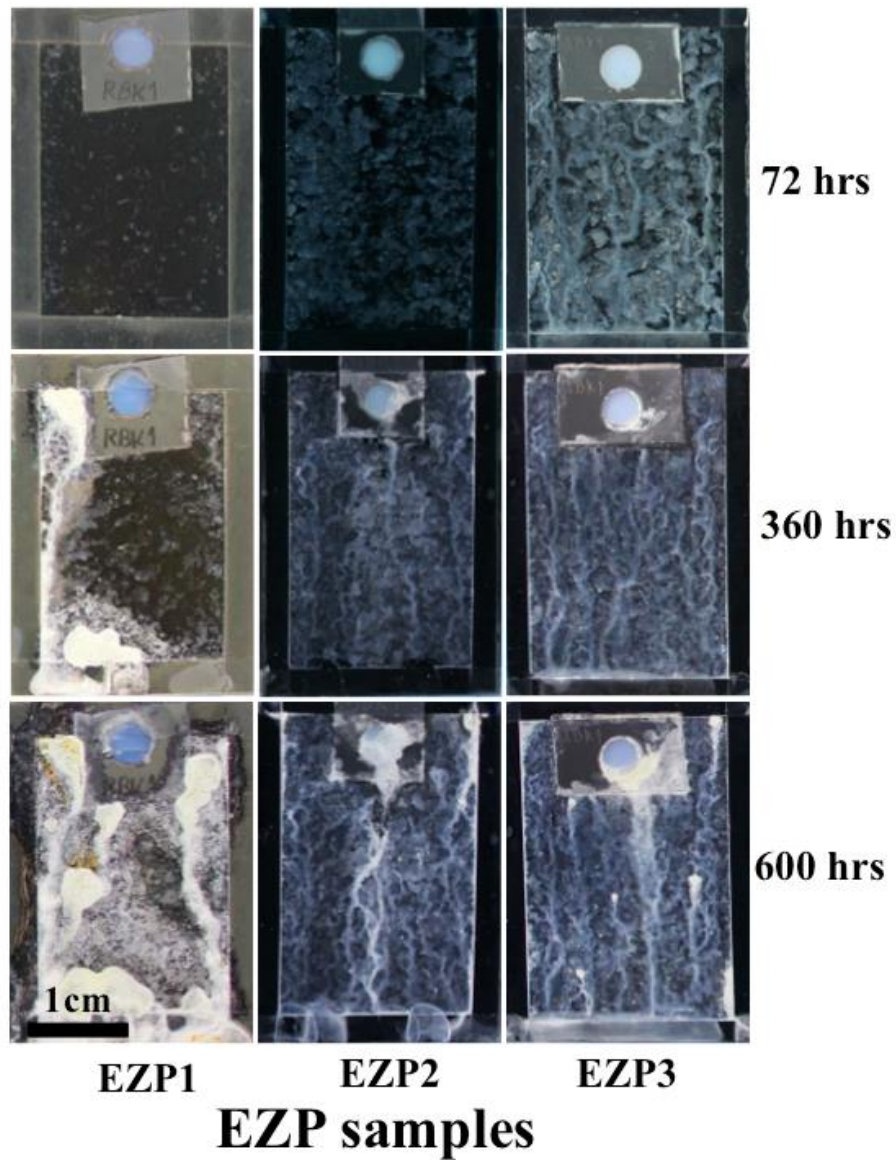


Figure 16 The appearance of the chromated electrogalvanized test specimens, EZP1, EZP2, and EZP3, following the salt spray test at different periods.

4.2.4 Relationship between structure and corrosion behavior of EZP

As presented in the results section, the specimens EZP1, EZP2, and EZP3 show distinct surface morphology and different microstructural details in their multi-layered passivation films. Interestingly, these structural and possibly chemical differentiations in the chromate conversion layers arise despite our having employed the same chromate treatment protocol on the three groups of electrogalvanized specimens. This may be rationalized through the formation mechanism of a chromate conversion coating layer, whereby the oxidation-reduction processes of the zinc dissolution and complex chromium compound film formation steps take place concurrently [116-120]. Since the surface metal of the electrogalvanized layer directly interacts with chromic acid and chromium salt solutions, it is reasonable that the crystallographic characteristic of the zinc layer would influence the development of the CCC layer. In this regard, it appears that the zinc layers with {110} texture promote the formation of the amorphous-oxide layer, whereas those with {100} texture facilitate an amorphous layer.

Considering the corrosion tests of the EZP specimens, the results from both the potentiodynamic polarization and salt spray tests show that the chromate layers serve as effective protective barriers [73, 121, 122], exhibiting much higher corrosion resistance than the unpassivated electrogalvanized (EZ) specimens. Furthermore, both sets of corrosion tests point to the relatively high corrosion resistance of specimens EZP2 and EZP3, as compared to EZP1. The results thus appear to suggest that a formation of a relatively thick amorphous-oxide layer comprising large grain structure, as induced by surface texture of zinc, helps promote the incremental

corrosion resistance benefit of the chromate films. Additionally, considering the variation of the polarization profiles in the anodic regions of the EZP specimens, the structure and surface morphology of the chromate layer may also influence the development of passive films during corrosion and provide an enhancement of corrosion resistance.

Part III. The feasibility of graphene as a potential for protecting corrosion

4.3.1 Surface morphology

Graphene electrolyte was plated onto the steel substrate. Figure 17 shows the surface morphology of the specimens analyzed by SEM: (a) and (b) are the micrograph of the steel substrate while, (c) and (d) are the micrograph of the graphene-based coatings. The graphene nanoplatelets were coated onto the steel substrate (Fig. 17(d)), which present the well-leveled and uniform generally. It was appeared to be successfully to coat graphene onto the steel substrate via this methodology (3.3.1 Sample fabrication).

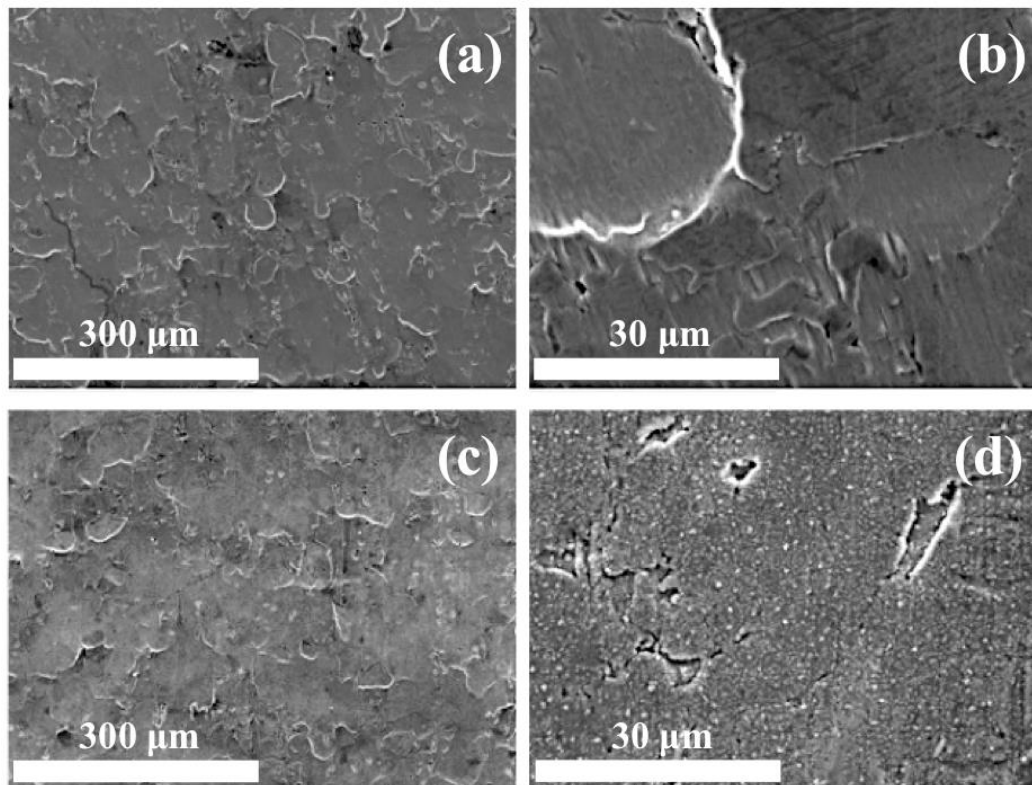
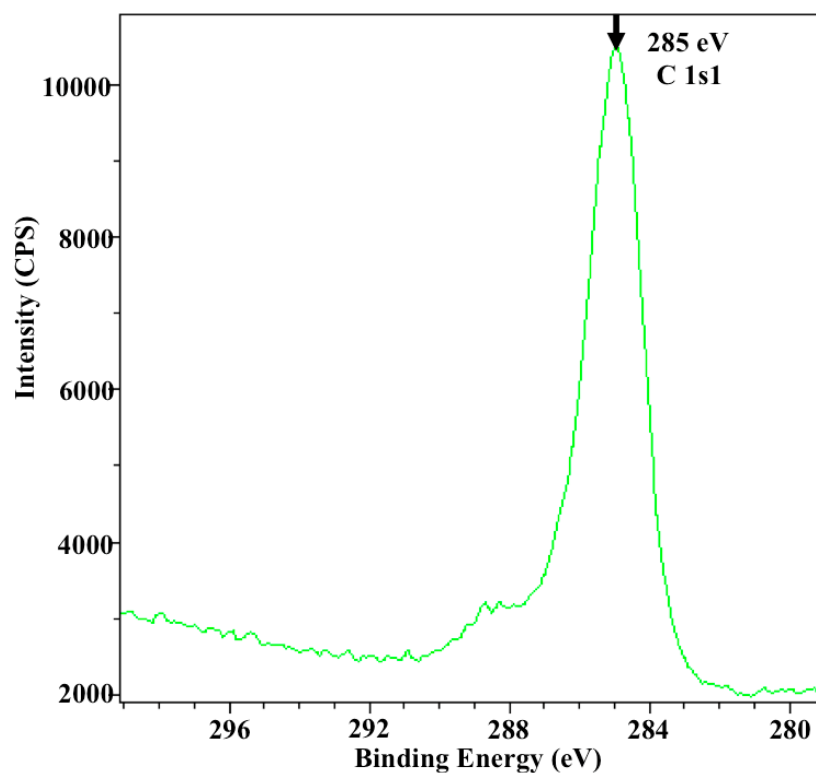


Figure 17 The surface morphology of the specimens. (a) and (b) are the micrograph of the steel substrate under the magnify of 200X and 2,000X, respectively. (c) and (d) are the micrograph of the graphene coatings under the magnify of 200X and 2,000X, respectively.

4.3.2 Surface structure



Peak	Position BE (eV)	FWHM (eV)	Raw Area (CPS)	RSF	Atomic Mass	Atomic Conc %	Mass Conc %
O 1s1	532.000	2.382	12901.5	2.850	15.999	19.30	24.12
O 1s2	533.800	1.194	279.1	2.850	15.999	0.42	0.52
O 1s3	533.100	0.448	31.9	2.850	15.999	0.05	0.06
C 1s1	285.000	1.846	16051.7	1.000	12.011	68.42	64.21
C 1s2	286.700	2.977	2185.7	1.000	12.011	9.32	8.74
C 1s3	288.700	1.298	585.7	1.000	12.011	2.50	2.34

Figure 18 Chemical structure of the graphene-base coating, which was analyzed under X-ray photoelectron spectrometer (XPS). The binding energy of graphene structure is 285 eV at peak c1s1.

The chemical structure and the phase confirmation of the coatings were carried out by XPS technique. Fig. 18 reveals the high peak intensity at binding energy of 285 eV, which is the representative of graphene phase. Therefore, the coatings were formed the graphene structure via this methodology (3.3.1 Sample fabrication).

4.3.3 Through-thickness structure

The plating parameter, which controlled the thickness, includes current density and deposited time. Figure 19 shows the surface morphology of graphene-based coatings in difference of current densities. The current density at 2 A/dm² presents the grey surface at the deposited time of 10 min and subsequently black surface (completely dark) at the deposited time of 20 min. While the 1 A/dm² presents the grey surface at the deposited time of 30 min. The higher current density (2 A/dm²) leads to the higher thickness. The graphene nanoplatelets were coated onto the substrate with high rate and formed coating faster than the lower current density (1 A/dm²). On the other hand, the deposited time presents the increasing of thickness with the deposited time increases.

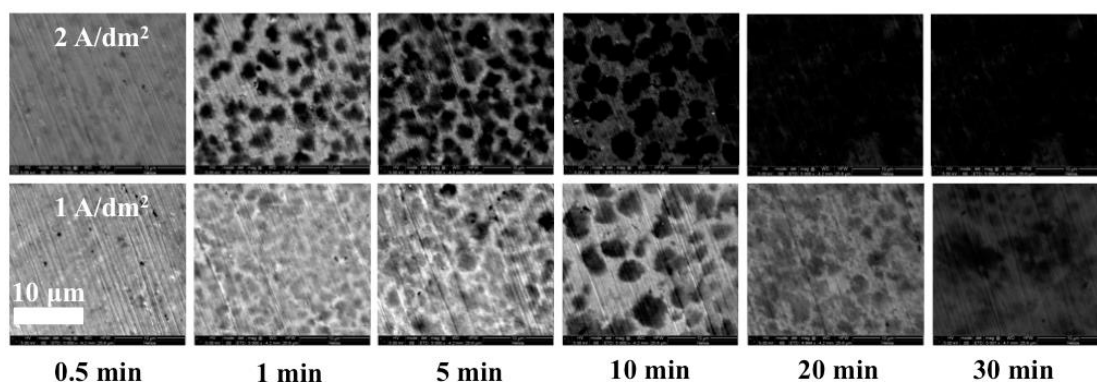


Figure 19 SEM micrographs showing surface morphology of the graphene-based coatings. The upper micrographs present the graphene coatings under current density of 2 A/dm^2 with increase the deposition time. The lower micrographs present the graphene coatings under current density of 1 A/dm^2 with increase the deposition time.

It is difficult to find the thickness of graphene coating due to the very thin layer in the scale of nanometer. However, this work employed FIB for cross sectioning the coating. Figure 20. displays the thickness of graphene-based coating in cross-section prepared by FIB technique. The coating thickness of the sample under 2 A/dm^2 with deposited time for 30 min was approximately 80 nm, which was the thickness of the high current density and long deposited time.

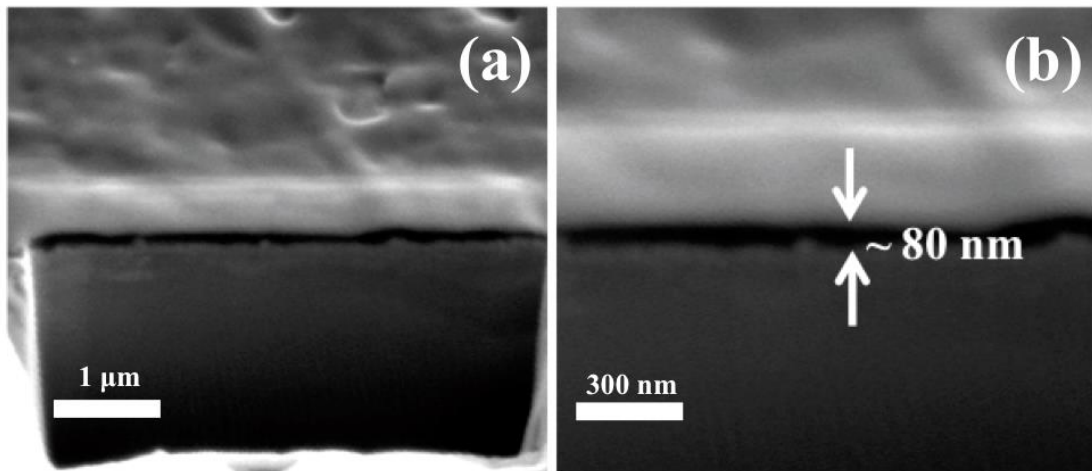


Figure 20 SEM Micrographs showing the cross-section prepared by FIB technique. (a) is the the thickness of graphene-based coating. (b) is the high magnify micrograph which presents the thickness of graphene approximately 80 nm.

4.3.4 Corrosion behavior of graphene-based coatings

4.3.4.1 Potentiodynamic polarization scan

Corrosion behavior of graphene-based coating was analyzed by potentiodynamic polarization. Figure 21 shows tafel plots of the specimens, including graphene-based coating (G/STEEL), steel substrate (STEEL), electrodeposited zinc (EZ), graphene coated zinc (G/EZ), electrodeposited zinc with chromate passivation (EZP). Based on the values of the corrosion currents (I_{corr}), the corrosion rates (CR) of these samples vary somewhat, ranging from 0.353, 0.300, 0.150, 0.033 and 0.001 mm/year for EZ, STEEL, G/EZ, G/STEEL, and EZP, respectively. Graphene coating presents the better corrosion resistance than others.

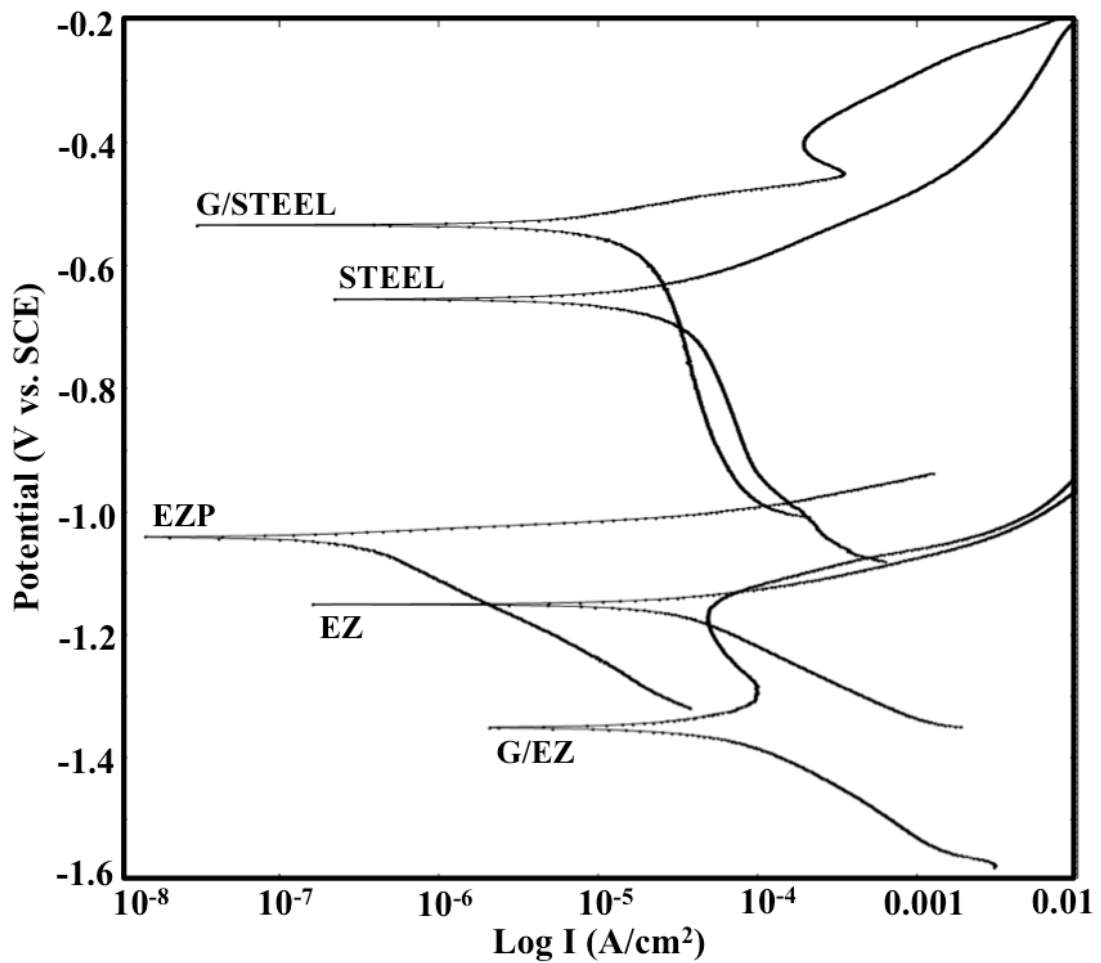


Figure 21 Tafel plots of the specimens, including graphene-based coating (G/STEEL), steel substrate (STEEL), electrodeposited zinc (EZ), graphene coated zinc (G/EZ), electrodeposited zinc with chromate passivation (EZP).

4.3.4.2 The accelerated corrosion test

The other test is the accelerated corrosion, which performed under the condition of 2-day immersion in 50 wt.% in NaCl. Figure 22 shows the digital images of the specimens before and after 2-day immersion in 50 wt.% in NaCl: (a) and (b) are the steel substrate and (c) and (d) are the graphene-based coatings.

Graphene coating has lower corrosion area (red rust) mean that it has higher corrosion resistance than steel substrate.

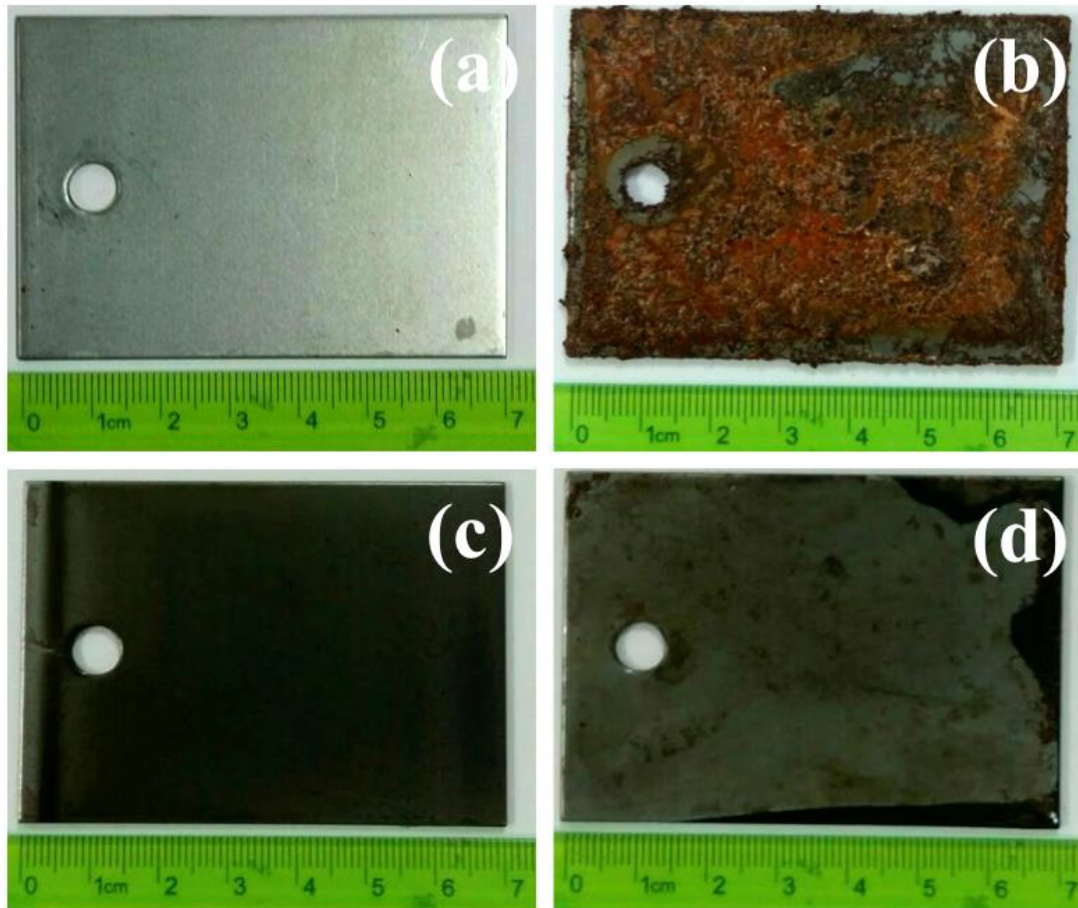


Figure 22 The digital images of the specimens before and after 2-day immersion in 50 wt.% in NaCl: (a) and (b) are the steel substrate and (c) and (d) are the graphene-based coatings.

CHAPTER VI CONCLUSION

This study investigates the relationship between microstructure and corrosion properties of both chromated and non-chromated electrogalvanized zinc coatings prepared with alkaline non-cyanide electrolytes containing three different sets of additives, namely a mixture of imidazole and epihalohydrin, polyquaternary amine salt, and polyethyleneimine. These additives significantly influence the crystallographic texture of zinc and in turn control the corrosion behaviors of the deposits. Therefore, the conclusion was divided into three parts below:

Part I. The processing-structure-property relationships in electrodeposited zinc

The investigation results indicate that crystallographic texture of zinc largely controls corrosion of the galvanized coatings, and decreasing of a texture coefficient of {100} planes contributes to improvements of corrosion resistance, as observed from the electrochemical analysis. The detailed examination provided by the FIB and TEM studies and the salt spray tests evidently points to the effects of interfacial voids, which is again induced by the plating additives, also critically affect the coatings' corrosion resistance.

Part II. The effects of the electrodeposited-zinc structure on the structure of chromium-trivalence passivation

The uses of different plating additives also distinctly affects the microstructural developments of the chromate conversion coating. Polyquaternary amine salt is identified as an especially effective additive for zinc plating in that it indirectly promotes formation of a relatively thick amorphous-oxide layer comprising large grain structure in the chromate film, which exhibits relatively high resistance to corrosion.

Part III. The feasibility of graphene as a potential for protecting corrosion

Graphene nanoplatelets were coated onto the steel substrate for protecting corrosion. The process to coat graphene is electrophoretic deposition which used current to induce the charged-graphene attached to the steel surface. Two feasibility studies for graphene-based coatings were identified: i) the feasibility of process for depositing graphene onto a steel substrate, which was emphasized on the additive, current density, and deposited time. ii) the feasibility of corrosion resistant property of the graphene-based coating. This study selected polyquaternary amine salt as an additive to synthesis the electrolyte, which had the high charge density (5.3 meq/mg). The additive plays an important role to increase the efficiency of deposit rate because graphene gained the cation from additive to form the conductive electrolyte. The high current density in the process (2 A/dm^2) increased the deposition rate. In addition, the high deposited time leads to increase thickness of graphene-based coatings. Therefore, two feasibility studies were identified. The coatings were confirmed for

the graphene coatings via SEM and XPS, with the surface morphology and surface structure analyses, respectively. In addition, the thickness of the coating was investigated via FIB and TEM. Moreover, graphene-based coating presents the better corrosion resistance than steel substrate and electrodeposited zinc (EZ). As the protective coatings of graphene it presents corrosion resistant behavior in both potentiodynamics and the accelerated corrosion test.



REFERENCES



- [1] B. Zhang, C. He, C. Wang, P. Sun, F. Li, and Y. Lin, "Synergistic corrosion inhibition of environment-friendly inhibitors on the corrosion of carbon steel in soft water," *Corrosion Science*, vol. 94, pp. 6-20, 5// 2015.
- [2] G. A. Zhang, N. Yu, L. Y. Yang, and X. P. Guo, "Galvanic corrosion behavior of deposit-covered and uncovered carbon steel," *Corrosion Science*, vol. 86, pp. 202-212, 9// 2014.
- [3] M. Narozny, K. Zakowski, and K. Darowicki, "Method of sacrificial anode transistor-driving in cathodic protection system," *Corrosion Science*, vol. 88, pp. 275-279, 11// 2014.
- [4] I. S. Cole, W. D. Ganther, S. A. Furman, T. H. Muster, and A. K. Neufeld, "Pitting of zinc: Observations on atmospheric corrosion in tropical countries," *Corrosion Science*, vol. 52, pp. 848-858, 3// 2010.
- [5] M. Yamashita and H. Uchida, "Recent research and development in solving atmospheric corrosion problems of steel industries in Japan," in *Industrial Applications of the Mössbauer Effect*, ed: Springer, 2002, pp. 153-166.
- [6] C. G. Munger and L. D. Vincent, "Corrosion prevention by protective coatings," 1999.
- [7] M. Yamashita, H. Miyuki, Y. Matsuda, H. Nagano, and T. Misawa, "The long term growth of the protective rust layer formed on weathering steel by atmospheric corrosion during a quarter of a century," *Corrosion Science*, vol. 36, pp. 283-299, 1994.
- [8] L. A. Roudabush, H. E. Townsend, and D. C. McCune, "Update on the Development of an Improved Cosmetic Corrosion Test by the Automotive and Steel Industries," SAE Technical Paper1993.
- [9] H. E. Townsend, "Status of a cooperative effort by the automotive and steel industries to develop a standard accelerated corrosion test," SAE Technical Paper1989.
- [10] R. A. Lula, "Corrosion resistant tube assembly," ed: Google Patents, 1983.
- [11] N. Kitashima, N. Takahashi, J. Ishiguro, and S. Kawamura, "Coating metal for preventing the crevice corrosion of austenitic stainless steel and method of preventing crevice corrosion using such metal," ed: Google Patents, 1982.
- [12] Z. Matilda, "Corrosion resistance of zinc electrodeposited from acidic and alkaline electrolytes using pulse current," *Chemical Papers*, vol. 63, pp. 574-578, 2009.
- [13] L. Veleva, M. Acosta, and E. Meraz, "Atmospheric corrosion of zinc induced by runoff," *Corrosion Science*, vol. 51, pp. 2055-2062, 9// 2009.
- [14] J. Morales, F. Díaz, J. Hernández-Borges, S. González, and V. Cano, "Atmospheric corrosion in subtropical areas: Statistic study of the corrosion of zinc plates exposed to several atmospheres in the province of Santa Cruz de Tenerife (Canary Islands, Spain)," *Corrosion Science*, vol. 49, pp. 526-541, 2// 2007.
- [15] G. Injeti, B. Leo, "Electrodeposition of nanostructured coatings and their characterization—a review," *Science and Technology of Advanced Materials*, vol. 9, 2008.
- [16] G. D. Wilcox and D. R. Gabe, "Electrodeposited zinc alloy coatings," *Corrosion Science*, vol. 35, pp. 1251-1258, // 1993.

- [17] H. Gleiter, "Nanocrystalline materials," *Progress in Materials Science*, vol. 33, pp. 223-315, 1989/01/01 1989.
- [18] G. Injeti and B. Leo, "Electrodeposition of nanostructured coatings and their characterization—a review," *Science and Technology of Advanced Materials*, vol. 9, p. 043001, 2008.
- [19] N. Jantaping, C. Banjongprasert, T. Chairuang Sri, U. Patakham, and Y. Boonyongmaneerat, "Challenges and strategies of surface modification of electrogalvanized coatings for electron microscopy analysis," *Micron*, vol. 86, pp. 48-53, 7// 2016.
- [20] R. Y. Wang, D. W. Kirk, and G. X. Zhang, "Effects of deposition conditions on the morphology of zinc deposits from alkaline zincate solutions," *Journal of The Electrochemical Society*, vol. 153, pp. C357-C364, 2006.
- [21] S. Khorsand, K. Raeissi, and M. A. Golozar, "An investigation on the role of texture and surface morphology in the corrosion resistance of zinc electrodeposits," *Corrosion Science*, vol. 53, pp. 2676-2678, 8// 2011.
- [22] R. Ramanauskas, R. Juškėnas, A. Kaliničenko, and L. F. Garfias-Mesias, "Microstructure and corrosion resistance of electrodeposited zinc alloy coatings," *Journal of Solid State Electrochemistry*, vol. 8, pp. 416-421, 2004// 2004.
- [23] R. Ramanauskas, L. Gudavičiūtė, R. Juškėnas, and O. Ščit, "Structural and corrosion characterization of pulse plated nanocrystalline zinc coatings," *Electrochimica Acta*, vol. 53, pp. 1801-1810, 12/31/ 2007.
- [24] G. Meng, L. Zhang, Y. Shao, T. Zhang, and F. Wang, "Study of the electrochemical behaviour of nanocrystalline zinc by statistical methods," *Corrosion Science*, vol. 51, pp. 1685-1689, 8// 2009.
- [25] H. Park and J. A. Szpunar, "The role of texture and morphology in optimizing the corrosion resistance of zinc-based electrogalvanized coatings," *Corrosion Science*, vol. 40, pp. 525-545, 1998/04/01 1998.
- [26] M. Mouanga, L. Ricq, J. Douglade, and P. Berçot, "Effects of some additives on the corrosion behaviour and preferred orientations of zinc obtained by continuous current deposition," *Journal of Applied Electrochemistry*, vol. 37, pp. 283-289, 2007// 2007.
- [27] M. S. Chandrasekar, Shanmugasigamani, and P. Malathy, "Synergetic effects of pulse constraints and additives in electrodeposition of nanocrystalline zinc: Corrosion, structural and textural characterization," *Materials Chemistry and Physics*, vol. 124, pp. 516-528, 11/1/ 2010.
- [28] R. F. Ashton and M. T. Hepworth, "Effect of crystal orientation on the anodic polarization and passivity of zinc," *Corrosion*, vol. 24, pp. 50-53, 1968.
- [29] R. Ramanauskas, P. Quintana, L. Maldonado, R. Pomés, and M. A. Pech-Canul, "Corrosion resistance and microstructure of electrodeposited Zn and Zn alloy coatings," *Surface and Coatings Technology*, vol. 92, pp. 16-21, 1997/06/01 1997.
- [30] R. Ramanauskas, "Structural factor in Zn alloy electrodeposit corrosion," *Applied Surface Science*, vol. 153, pp. 53-64, 12// 1999.
- [31] ASTM, "Standard Specification for Electrodeposited Coatings of Zinc on Iron and Steel," *ASTM*, vol. B 633-98, p. 5.

- [32] K. M. S. Youssef, C. C. Koch, and P. S. Fedkiw, "Improved corrosion behavior of nanocrystalline zinc produced by pulse-current electrodeposition," *Corrosion Science*, vol. 46, pp. 51-64, 2004.
- [33] M. C. Li, L. L. Jiang, W. Q. Zhang, Y. H. Qian, S. Z. Luo, and J. N. Shen, "Electrodeposition of nanocrystalline zinc from acidic sulfate solutions containing thiourea and benzalacetone as additives," *Journal of Solid State Electrochemistry*, vol. 11, pp. 549-553, 2007.
- [34] M. Cai and S. M. Park, "Oxidation of zinc in alkaline solutions studied by electrochemical impedance spectroscopy," *Journal of the Electrochemical Society*, vol. 143, pp. 3895-3902, 1996.
- [35] D. C. W. Kannangara and B. E. Conway, "Zinc oxidation and redeposition processes in aqueous alkali and carbonate solutions I. pH and carbonate ion effects in film formation and dissolution," *Journal of The Electrochemical Society*, vol. 134, pp. 894-906, 1987.
- [36] C. V. Bishop, R. Vogel, J. R. Kochilla, and C. Wennefors, "Corrosion resistant films from trivalent chrome based solutions applied to electrodeposited zinc and zinc alloys," p. 355.
- [37] A. K. Geim and K. S. Novoselov, "The rise of graphene," *Nat Mater*, vol. 6, pp. 183-191, 03//print 2007.
- [38] Y. Liu, B. Xie, Z. Zhang, Q. Zheng, and Z. Xu, "Mechanical properties of graphene papers," *Journal of the Mechanics and Physics of Solids*, vol. 60, pp. 591-605, 2012.
- [39] I. W. Frank, D. M. Tanenbaum, A. M. Van der Zande, and P. L. McEuen, "Mechanical properties of suspended graphene sheets," *Journal of Vacuum Science & Technology B*, vol. 25, pp. 2558-2561, 2007.
- [40] S. Bohm, "Graphene against corrosion," *Nat Nano*, vol. 9, pp. 741-742, 10//print 2014.
- [41] W. Zhang, S. Lee, K. L. McNear, T. F. Chung, S. Lee, K. Lee, *et al.*, "Use of graphene as protection film in biological environments," *Scientific reports*, vol. 4, 2014.
- [42] H. E. Townsend, R. D. Granata, D. C. McCune, W. A. Schumacher, and R. J. Neville, "Progress by the automotive and steel industries toward an improved laboratory cosmetic corrosion test," SAE Technical Paper1991.
- [43] D. Daoud, T. Douadi, H. Hamani, S. Chafaa, and M. Al-Noaimi, "Corrosion inhibition of mild steel by two new S-heterocyclic compounds in 1 M HCl: Experimental and computational study," *Corrosion Science*, vol. 94, pp. 21-37, 5// 2015.
- [44] A. R. Marder, "The metallurgy of zinc-coated steel," *Progress in Materials Science*, vol. 45, pp. 191-200, 2000.
- [45] A. G. A., "Zinc Coatings," *American Galvanizers Association*, 2000.
- [46] T. Watanabe, "NANO-PLATING Microstructure Control Theory of Plated Film and Data Base of Plated Film Microstructure," *Elsevier Ltd*, 2004.
- [47] M. Paunovic, M. Schlesinger, "Fundamentals of Electrochemical Deposition," *A JOHN WILEY & SONS, INC., PUBLICATION*, pp. 8-9, 2006.
- [48] K. Saber, C. C. Koch, P. S. Fedkiw, "Pulse current electrodeposition of nanocrystalline zinc," *Materials Science and Engineering A*, vol. 341, pp. 174-181, 2003.

- [49] K. O. Nayana, T. V. Venkatesha "Synergistic effects of additives on morphology, texture and discharge mechanism of zinc during electrodeposition," *Journal of Electroanalytical Chemistry*, vol. 663, pp. 98-107, 2011.
- [50] F. W. Joseph, "Bright zinc plating," ed: Google Patents, 1948.
- [51] H. Nakano, S. Oue, S. Taniguchi, S. Kobayashi, H. Fukushima, "Effects of Small Amounts of Mo W Sn Additives on the Morphology and Orientation of electrodeposited Zinc," *ISIJ International*, vol. 48, pp. 634-639, 2008.
- [52] Y. M. Jose´ Luis Ortiz-Aparicio, Thomas W. Chapman, Rau´ l Ortega, Eric Chainet, "Electrodeposition of zinc in the presence of quaternary ammonium compounds from alkaline chloride bath," *J Appl Electrochem*, vol. 45, p. 12, 2015.
- [53] L. R. M. Mouanga., J. Douglade., P. Berçot., "Corrosion behaviour of zinc deposits obtained under pulse current electrodeposition-Effects of coumarin as additive," *Corrosion Science*, vol. 51, p. 9, 2009.
- [54] M. Mouanga, L. Ricq, G. Douglade, J. Douglade, P. Berçot, "Influence of coumarin on zinc electrodeposition," *Surface and Coatings Technology*, vol. 201, pp. 762-767, 2006.
- [55] B. Kavitha, P. Santhosh, M. Renukadevi, A. Kalpana, P. Shakkthivel, and T. Vasudevan, "Role of organic additives on zinc plating," *Surface and Coatings Technology*, vol. 201, pp. 3438-3442, 12/4/ 2006.
- [56] C.-C. H. Ju-Cheng Hsieh, Tai-Chou Lee, "Effects of polyamines on the deposition behavior and morphology of zinc electroplated at high-current densities in alkaline cyanide-free baths," *Surface & Coatings Technology*, vol. 203, p. 6, 2009.
- [57] M. S. Chandrasekar, Shanmugasigamani, M. Pushpavanam, "Synergetic effects of pulse constraints and additives in electrodeposition of nanocrystalline zinc: Corrosion, structural and textural characterization," *Materials Chemistry and Physics*, vol. 124, pp. 516-528, 2010.
- [58] M. Guozhe, Z. Lei, S. Yawei, Z. Tao, W. Fuhui, "Study of the electrochemical behaviour of nanocrystalline zinc by statistical methods," *Corrosion Science*, vol. 51, pp. 1685-1689, 2009.
- [59] R. Y. Wang, D. W. Kirk, G. X. Zhang, "Effects of Deposition Conditions on the Morphology of Zinc Deposits from Alkaline Zincate Solutions," *Journal of The Electrochemical Society*, vol. 153, p. C357, 2006.
- [60] K. Raeissi, A. Saatchi, and M. A. Golozar, "Effect of nucleation mode on the morphology and texture of electrodeposited zinc," *Journal of applied electrochemistry*, vol. 33, pp. 635-642, 2003.
- [61] S. Khorsand, K. Raeissi, M. A. Golozar, "An investigation on the role of texture and surface morphology in the corrosion resistance of zinc electrodeposits," *Corrosion Science*, vol. 53, pp. 2676-2679, 2011.
- [62] O. B. Girin, Panasenko, S.A., "Effect of the texture of electrolytic zinc coatings on their corrosion resistance," *Zashch. Met.*, vol. 25, p. 3, 1989.
- [63] R. Ramanauskas, R. Juškėnas, A. Kaliničenko, L. F. Garfias-Mesias, "Microstructure and corrosion resistance of electrodeposited zinc alloy coatings," *Journal of Solid State Electrochemistry*, vol. 8, pp. 416-421, 2003.

- [64] M. Mouanga, L. Ricq, J. Douglade, P. Berçot, "Effects of some additives on the corrosion behaviour and preferred orientations of zinc obtained by continuous current deposition," *Journal of Applied Electrochemistry*, vol. 37, pp. 283-289, 2006.
- [65] F. W. Eppensteiner and M. R. Jenkind, "Chromate conversion coatings," *Metal Finishing*, vol. 105, pp. 413-424, // 2007.
- [66] D. L. Snyder, "Decorative chromium plating," *Metal Finishing*, vol. 99, Supplement 1, pp. 215-222, 1// 2001.
- [67] M. Branstead and C. Bieler, "Trivalent chromium for a new generation," *Metal Finishing*, vol. 107, pp. 27-33, 1// 2009.
- [68] N. Zaki, "Trivalent chrome conversion coating for zinc and zinc alloys," *Metal Finishing*, vol. 105, pp. 425-435, // 2007.
- [69] N. Zaki, "Trivalent chrome conversion coating for zinc and zinc alloys," *Metal Finishing*, vol. 100, Supplement 1, pp. 492-501, 1// 2002.
- [70] M. P. Gigandet, J. Faucheu, and M. Tachez, "Formation of black chromate conversion coatings on pure and zinc alloy electrolytic deposits: role of the main constituents," *Surface and Coatings Technology*, vol. 89, pp. 285-291, 1997.
- [71] C. R. Tomachuk, C. I. Elsner, A. R. Di Sarli, and O. B. Ferraz, "Corrosion resistance of Cr(III) conversion treatments applied on electrogalvanised steel and subjected to chloride containing media," *Materials Chemistry and Physics*, vol. 119, pp. 19-29, 1/15/ 2010.
- [72] M. Hosseini, H. Ashassi-Sorkhabi, and H. A. Y. Ghiasvand, "Corrosion Protection of Electro-Galvanized Steel by Green Conversion Coatings," *Journal of Rare Earths*, vol. 25, pp. 537-543, 10// 2007.
- [73] T. Bellezze, G. Roventi, and R. Fratesi, "Electrochemical study on the corrosion resistance of Cr III-based conversion layers on zinc coatings," *Surface and Coatings Technology*, vol. 155, pp. 221-230, 6/17/ 2002.
- [74] F. W. Eppensteiner and M. R. Jenkins, "Chromate conversion coatings," *Metal Finishing*, vol. 98, pp. 497-509, 1// 2000.
- [75] F. I. Danilov, V. S. Protsenko, V. O. Gordiienko, S. C. Kwon, J. Y. Lee, and M. Kim, "Nanocrystalline hard chromium electrodeposition from trivalent chromium bath containing carbamide and formic acid: Structure, composition, electrochemical corrosion behavior, hardness and wear characteristics of deposits," *Applied Surface Science*, vol. 257, pp. 8048-8053, 7/1/ 2011.
- [76] W.-K. Chen, C.-Y. Bai, C.-M. Liu, C.-S. Lin, and M.-D. Ger, "The effect of chromic sulfate concentration and immersion time on the structures and anticorrosive performance of the Cr(III) conversion coatings on aluminum alloys," *Applied Surface Science*, vol. 256, pp. 4924-4929, 6/1/ 2010.
- [77] G. Meng, L. Zhang, Y. Shao, T. Zhang, F. Wang, C. Dong, *et al.*, "Effect of refining grain size on the corrosion behavior of Cr(III) conversion layers on zinc coatings," *Scripta Materialia*, vol. 61, pp. 1004-1007, 12// 2009.
- [78] Y.-T. Chang, N.-T. Wen, W.-K. Chen, M.-D. Ger, G.-T. Pan, and T. C.-K. Yang, "The effects of immersion time on morphology and electrochemical properties of the Cr(III)-based conversion coatings on zinc coated steel surface," *Corrosion Science*, vol. 50, pp. 3494-3499, 12// 2008.

- [79] Y. B. Song and D. T. Chin, "Current efficiency and polarization behavior of trivalent chromium electrodeposition process," *Electrochimica Acta*, vol. 48, pp. 349-356, 12/20/ 2002.
- [80] N.-T. Wen, C.-S. Lin, C.-Y. Bai, and M.-D. Ger, "Structures and characteristics of Cr(III)-based conversion coatings on electrogalvanized steels," *Surface and Coatings Technology*, vol. 203, pp. 317-323, 11/25/ 2008.
- [81] K. Cho, V. S. Rao, and H. Kwon, "Microstructure and electrochemical characterization of trivalent chromium based conversion coating on zinc," *Electrochimica Acta*, vol. 52, pp. 4449-4456, 2007.
- [82] K. Cho, V. Shankar Rao, and H. Kwon, "Microstructure and electrochemical characterization of trivalent chromium based conversion coating on zinc," *Electrochimica Acta*, vol. 52, pp. 4449-4456, 3/20/ 2007.
- [83] R. Berger, U. Bexell, T. Mikael Grehk, and S.-E. Hörnström, "A comparative study of the corrosion protective properties of chromium and chromium free passivation methods," *Surface and Coatings Technology*, vol. 202, pp. 391-397, 11/25/ 2007.
- [84] X. Zhang, C. van den Bos, W. G. Sloof, A. Hovestad, H. Terryn, and J. H. W. de Wit, "Comparison of the morphology and corrosion performance of Cr(VI)- and Cr(III)-based conversion coatings on zinc," *Surface and Coatings Technology*, vol. 199, pp. 92-104, 9/1/ 2005.
- [85] D. Prasai, J. C. Tuberquia, R. R. Harl, G. K. Jennings, and K. I. Bolotin, "Graphene: corrosion-inhibiting coating," *ACS nano*, vol. 6, pp. 1102-1108, 2012.
- [86] N. T. Kirkland, T. Schiller, N. Medhekar, and N. Birbilis, "Exploring graphene as a corrosion protection barrier," *Corrosion Science*, vol. 56, pp. 1-4, 2012.
- [87] C.-H. Chang, T.-C. Huang, C.-W. Peng, T.-C. Yeh, H.-I. Lu, W.-I. Hung, *et al.*, "Novel anticorrosion coatings prepared from polyaniline/graphene composites," *Carbon*, vol. 50, pp. 5044-5051, 2012.
- [88] Y. Jiang, X. Zhang, C. Shan, S. Hua, Q. Zhang, X. Bai, *et al.*, "Functionalization of graphene with electrodeposited Prussian blue towards amperometric sensing application," *Talanta*, vol. 85, pp. 76-81, 2011.
- [89] L. Chen, Y. Tang, K. Wang, C. Liu, and S. Luo, "Direct electrodeposition of reduced graphene oxide on glassy carbon electrode and its electrochemical application," *Electrochemistry Communications*, vol. 13, pp. 133-137, 2011.
- [90] C. Liu, K. Wang, S. Luo, Y. Tang, and L. Chen, "Direct Electrodeposition of Graphene Enabling the One- Step Synthesis of Graphene-Metal Nanocomposite Films," *Small*, vol. 7, pp. 1203-1206, 2011.
- [91] S. Chen, L. Brown, M. Levendorf, W. Cai, S.-Y. Ju, J. Edgeworth, *et al.*, "Oxidation resistance of graphene-coated Cu and Cu/Ni alloy," *ACS nano*, vol. 5, pp. 1321-1327, 2011.
- [92] M. Hilder, B. Winther-Jensen, D. Li, M. Forsyth, and D. R. MacFarlane, "Direct electro-deposition of graphene from aqueous suspensions," *Physical Chemistry Chemical Physics*, vol. 13, pp. 9187-9193, 2011.
- [93] R. S. Sundaram, C. Gómez- Navarro, K. Balasubramanian, M. Burghard, and K. Kern, "Electrochemical modification of graphene," *Advanced Materials*, vol. 20, pp. 3050-3053, 2008.

- [94] L. Besra and M. Liu, "A review on fundamentals and applications of electrophoretic deposition (EPD)," *Progress in Materials Science*, vol. 52, pp. 1-61, 1// 2007.
- [95] A. Chavez-Valdez, M. S. P. Shaffer, and A. R. Boccaccini, "Applications of Graphene Electrophoretic Deposition. A Review," *The Journal of Physical Chemistry B*, vol. 117, pp. 1502-1515, 2013/02/14 2013.
- [96] M. Diba, D. W. H. Fam, A. R. Boccaccini, and M. S. P. Shaffer, "Electrophoretic deposition of graphene-related materials: A review of the fundamentals," *Progress in Materials Science*, vol. 82, pp. 83-117, 9// 2016.
- [97] G. N. K. Ramesh Babu, G. Devaraj, and J. Ayyapparaj, "Studies on non-cyanide alkaline zinc electrolytes," *Journal of Solid State Electrochemistry*, vol. 3, pp. 48-51, 1998// 1998.
- [98] A. Y. Hosny, T. J. O'Keefe, and W. J. James, "Hull cell technique for evaluating zinc sulfate electrolytes," *Minerals Engineering*, vol. 2, pp. 415-423, 1989/01/01 1989.
- [99] L. F. G. Williams, "The initiation of corrosion of chromated zinc electroplate on steel," *Corrosion Science*, vol. 13, pp. 865-868, 1973/01/01 1973.
- [100] Y.-T. Chang, N.-T. Wen, W.-K. Chen, M.-D. Ger, G.-T. Pan, and T. C. K. Yang, "The effects of immersion time on morphology and electrochemical properties of the Cr (III)-based conversion coatings on zinc coated steel surface," *Corrosion Science*, vol. 50, pp. 3494-3499, 2008.
- [101] S. Thomas, N. Birbilis, M. S. Venkatraman, and I. S. Cole, "Self-repairing oxides to protect zinc: review, discussion and prospects," *Corrosion Science*, vol. 69, pp. 11-22, 2013.
- [102] F. Rosalbino, G. Scavino, G. Mortarino, E. Angelini, and G. Lunazzi, "EIS study on the corrosion performance of a Cr(III)-based conversion coating on zinc galvanized steel for the automotive industry," *Journal of Solid State Electrochemistry*, vol. 15, pp. 703-709, 2011// 2011.
- [103] P. Scherrer, "Estimation of the size and internal structure of colloidal particles by means of rC6ntgen," *Nachr. Ges. Wiss. GC6ttingen*, vol. 2, pp. 96-100, 1918.
- [104] P. R. Sere, J. D. Culcasi, C. I. Elsner, and A. R. Di Sarli, "Relationship between texture and corrosion resistance in hot-dip galvanized steel sheets," *Surface and Coatings Technology*, vol. 122, pp. 143-149, 1999.
- [105] J. T. Bonarski, "X-ray texture tomography of near-surface areas," *Progress in Materials Science*, vol. 51, pp. 61-149, 1// 2006.
- [106] L. A. Giannuzzi and F. A. Stevie, "A review of focused ion beam milling techniques for TEM specimen preparation," *Micron*, vol. 30, pp. 197-204, 6// 1999.
- [107] T. M. Jian Li, S. Dionne, "Recent advances in FIB-TEM specimen preparation techniques," *Materials Characterization*, vol. 57, p. 7, 2005.12.007 2006.
- [108] I. Aslam, B. Li, R. L. Martens, J. R. Goodwin, H. J. Rhee, and F. Goodwin, "Transmission electron microscopy characterization of the interfacial structure of a galvanized dual-phase steel," *Materials Characterization*, vol. 120, pp. 63-68, 10// 2016.

- [109] G. A. El-Mahdy, A. Nishikata, and T. Tsuru, "Electrochemical corrosion monitoring of galvanized steel under cyclic wet–dry conditions," *Corrosion Science*, vol. 42, pp. 183-194, 1// 2000.
- [110] J.-C. Hsieh, C.-C. Hu, and T.-C. Lee, "Effects of polyamines on the deposition behavior and morphology of zinc electroplated at high-current densities in alkaline cyanide-free baths," *Surface and Coatings Technology*, vol. 203, pp. 3111-3115, 7/15/ 2009.
- [111] J. Agrisuelas, J. Juan García-Jareño, D. Gimenez-Romero, and F. Vicente, "An electromechanical perspective on the metal/solution interfacial region during the metallic zinc electrodeposition," *Electrochimica Acta*, vol. 54, pp. 6046-6052, 10/30/ 2009.
- [112] K. O. Nayana and T. V. Venkatesha, "Synergistic effects of additives on morphology, texture and discharge mechanism of zinc during electrodeposition," *Journal of Electroanalytical Chemistry*, vol. 663, pp. 98-107, 12/15/ 2011.
- [113] G. Barcelo, M. Sarret, C. Müller, and J. Pregonas, "Corrosion resistance and mechanical properties of zinc electrocoatings," *Electrochimica Acta*, vol. 43, pp. 13-20, 1998.
- [114] N. R. Short, S. Zhou, and J. K. Dennis, "Electrochemical studies on the corrosion of a range of zinc alloy coated steel in alkaline solutions," *Surface and Coatings Technology*, vol. 79, pp. 218-224, 1996/02/01 1996.
- [115] X. Zhang, W. G. Sloof, A. Hovestad, E. P. M. van Westing, H. Terryn, and J. H. W. de Wit, "Characterization of chromate conversion coatings on zinc using XPS and SKPFM," *Surface and Coatings Technology*, vol. 197, pp. 168-176, 7/22/ 2005.
- [116] A. R. Di Sarli, J. D. Culcasi, C. R. Tomachuk, C. I. Elsner, J. M. Ferreira-Jr, and I. Costa, "A conversion layer based on trivalent chromium and cobalt for the corrosion protection of electrogalvanized steel," *Surface and Coatings Technology*, vol. 258, pp. 426-436, 2014.
- [117] L. M. Baugh and A. Higginson, "Passivation of zinc in concentrated alkaline solution—I. Characteristics of active dissolution prior to passivation," *Electrochimica Acta*, vol. 30, pp. 1163-1172, 1985.
- [118] M. Nikolova, O. Harizanov, P. Steftchev, I. Kristev, and S. Rashkov, "Black chromate conversion coatings on electrodeposited zinc," *Surface and Coatings Technology*, vol. 34, pp. 501-514, 1988.
- [119] M. J. Vasquez, G. P. Halada, and C. R. Clayton, "The application of synchrotron-based spectroscopic techniques to the study of chromate conversion coatings," *Electrochimica acta*, vol. 47, pp. 3105-3115, 2002.
- [120] N.-T. Wen, C.-S. Lin, C.-Y. Bai, and M.-D. Ger, "Structures and characteristics of Cr (III)-based conversion coatings on electrogalvanized steels," *Surface and Coatings Technology*, vol. 203, pp. 317-323, 2008.
- [121] M. R. El-Sharif, Y. J. Su, C. U. Chisholm, and A. Watson, "Corrosion resistance of electrodeposited zinc-chromium alloy coatings," *Corrosion science*, vol. 35, pp. 1259-1265, 1993.
- [122] A. A. O. Magalhães, I. C. P. Margarit, and O. R. Mattos, "Electrochemical characterization of chromate coatings on galvanized steel," *Electrochimica acta*, vol. 44, pp. 4281-4287, 1999.

APPENDIX

Micron 86 (2016) 1–6



Contents lists available at ScienceDirect

Micron

journal homepage: www.elsevier.com/locate/micron

Challenges and strategies of surface modification of electrogalvanized coatings for electron microscopy analysis



Narin Jantaping^a, Chaiyasit Banjongprasert^b, Torranin Chairuangsrri^c,
Ussadawut Patakham^d, Yuttanant Boonyongmaneerat^{e,*}

^a Nanoscience and Technology, Graduate School, Chulalongkorn University, Bangkok 10330, Thailand

^b Department of Physics and Materials Science, Faculty of Science, Chiang Mai University, Chiang Mai 50200, Thailand

^c Department of Industrial Chemistry, Faculty of Science, Chiang Mai University, Chiang Mai 50200, Thailand

^d National Metal and Materials Technology Center, National Science and Technology Development Agency, Pathumtani 12120, Thailand

^e Metallurgy and Materials Science Research Institute, Chulalongkorn University, Bangkok 10330, Thailand

ARTICLE INFO

Article history:

Received 3 February 2016

Received in revised form 18 April 2016

Accepted 18 April 2016

Available online 25 April 2016

Keywords:

Characterization

Electrogalvanizing

Metallography

Electrochemical polishing

Electron microscopy

ABSTRACT

Despite wide usage of electrogalvanized coatings in various applications, characterization studies on their micro/crystal structure, and the understanding of how they correspondingly affect the properties, such as corrosion, are rather limited. This is mainly attributed to some difficulties in preparing and examining the zinc coating layers, owing to their intrinsically low corrosion resistance and refined nano-scaled crystallite size. This study aims to examine such challenges systematically and propose some mitigation strategies. Particularly, sample preparation processes, including surface finishing for metallography and sample thinning processes are explored. Furthermore, a range of electron microscopy techniques, including scanning electron microscopy (SEM), electron back scattered diffractometry (EBSD), and transmission electron microscopy (TEM) are investigated in relation to the achievable clarity of microstructural details of electrogalvanized coatings.

© 2016 Elsevier Ltd. All rights reserved.

1. Introduction

Owing to good corrosion protection at moderate cost, ductility and formability, and a uniformly thin coating layer of electrodeposited zinc, also termed electrogalvanized coating, has been widely employed as a surface finish in various industrial applications, ranging from automotives, electronics, and households (Wilcox and Gabe, 1993; Marder, 2000; Muster and Cole, 2004; Crotty, 1996). The esteemed properties primarily result from chemistry of zinc and the coating's microstructure and crystallographic structure of coating (Ramanauskas et al., 1997; Morales et al., 2007; Chianpairot et al., 2011; Yoshioka et al., 1990; Winand, 1991; Eppensteiner and Jennkind, 2007; Zhang et al., 2005; Ramanauskas et al., 2007). While understanding its structure would provide effective channels to tailor and enhance the properties of electrogalvanized coating, in a major part, this is barred by delicate nature of metallic zinc with respect to surface preparation protocols required for microscopy examinations. This is evidenced by the presence of a very limited number of publications devoted to

metallographic studies of electrogalvanized coating (Raëissi et al., 2007; Wang et al., 2006) and consistent remarks on difficulties during sample preparation, including rapid surface oxidation, peel-off, and non-uniformity upon cutting, grinding, and surface polishing (Injeti and Leo, 2008; Zhang et al., 2014). Furthermore, the challenge is often escalated by a refinement of the coating structure in a nanometer scale, which necessitates distinguished surface preparation quality for advanced microscopy characterizations (Saber et al., 2003; Muralidhara and Arthoba Naik, 2008).

In the present study, surface preparation of the electrogalvanized coatings for advanced microscopy techniques, including field-emission electron microscopy (FE-SEM), electron back scattered diffractometry (EBSD), and transmission electron microscopy (TEM) are systematically examined. Particularly, the challenges encountered upon sample preparations for these techniques are deduced and corresponding strategies, including electropolishing, to mitigate the problems are proposed and investigated. Optimal outcomes obtained with the current study would specifically provide proper methodology for the electron microscopy of electrogalvanized coatings, and also shed some lights on possible surface preparation protocols for other types of galvanized and readily-oxidized coatings.

* Corresponding author.

E-mail address: yuttanant.b@chula.ac.th (Y. Boonyongmaneerat).

2. Surface preparation and characterization: challenge and strategies

2.1. Surface finishing for metallography

Two of the common techniques for examination of microstructural details of metal surfaces are scanning electron microscopy (SEM) and electron back scattered diffractometry (EBSD). While these two techniques commonly require highly planar and uniform conditions for the surface of the sample, there are some distinctive requirements which pertain to the usage and functions of the techniques, as follows:

2.1.1. SEM

Through the scanning of secondary or back-scattered electrons on interested areas, the SEM is commonly employed for analyzing the morphology and topography of materials in the scale of a few microns to nanometer. Three electron sources of the SEM, including tungsten-filament, LaB₆-crystal, and field-emission, are available, with the latter, also termed FE-SEM, providing the highest resolution (Exner and Weinbruch, 2004). Grain structure, granules, roughness, thickness, and cracks are among possible microstructural features of the electrogalvanized coating to be examined under the SEM.

Nevertheless, some basic challenges exist in its surface preparation process, which consists of (1) sample cutting, (2) mounting, (3) grinding, (4) polishing, and (5) etching (Aliya, 2004). Due to the intrinsic sacrificial nature of electrogalvanized coating, the major issues being faced are developments of surface non-uniformity in the polishing step and localized corrosion attack induced by chemical etchants of the last step which hinders visibility of the microstructural features. Whereas the first problem is commonly mitigated by using oil-based lubricants as polishing mediums (Samuels, 2003), the best practice for the latter issue remains unclear.

In the present study, 3 strategies to prepare the surface of electrogalvanized coating for microstructural examination under SEM were examined comparatively, including polishing with oil-based diamond suspension, final polishing with water based colloidal silica solution, and electropolishing with Spyridelis method. Whereas colloidal silica is a common polishing medium for Al, Cu, and Fe and exhibits mild etchant character, Spyridelis method which employs phosphoric acid in ethyl alcohol, has been adopted to etch thin sheets of zinc (Spyridelis, 1971).

2.1.2. EBSD

EBSD is the advanced technique for characterization of crystal orientations of a crystalline or polycrystalline material. Equipped in SEM, EBSD analyzes diffraction pattern generated from backscattered portion of electron beams and develops orientation mapping representing individual crystallographic planes that are present on materials' surfaces (Venables and Harland, 1973). To prepare samples for the EBSD analysis, perfectly clear and highly smooth surface, somewhat exceeding the tolerable quality of SEM samples, is required. Such challenge in sample preparation may therefore partly explain a very limited number of crystallographic studies of galvanized coatings.

For the most parts, the EBSD samples are prepared with the same steps as those for SEM samples, except that higher attention is to be paid on the uniformity and defect-free quality of the surface following polishing. Furthermore, minimally etched surface quality is merely needed. If structures of a substrate or a coating interface are to be characterized in concurrent to the coating, it is also important to control and balance the polishing and etching rates of the adjoined materials. Such process is often found difficult due to a relatively rapid polishing rate of metallic zinc.

In the present study, 2 strategies to prepare the surface of electrogalvanized coating for crystal structure examination with the EBSD were investigated, namely final polishing with water-based colloidal silica solution, and electropolishing with Adair method which employed perchloric acid in ethanol (Edington, 1975). These two methods were chosen as it was known that they could also polish the surface of steel substrates (Weidmann, 1985).

2.2. Sample thinning for TEM

TEM is the important characterizing technique for analyzing the microstructure and crystal structure of materials in the nanometer and angstrom regimes. Bright field mode allows analysis of grain structure and atomic arrangement, whereas the diffraction mode provides crystal orientations and observations of defects. Despite its powerful functions, TEM is known to be one of the hardest microscopy techniques to prepare a sample. Particularly, the sample needs to be thinned below 50–60 nm to allow electron to transmit through. Mechanical dimpling, ion milling, and electrochemical polishing are among possible processes to prepare exceptionally thin samples (Reimer, 2013)

Similar to EBSD, TEM studies of electrogalvanized coatings are very limited. Furthermore, a specific guideline for TEM sample preparation of the zinc-based coating is not available in publications. Spyridelis and Adair electrochemical polishing methods were comparatively chosen for examination herein with respect to clarity of TEM micrographs and corresponding diffraction patterns.

3. Experimental

3.1. Sample fabrication

A set of electrogalvanized specimens was prepared by the electrodeposition process using the environmentally friendly alkaline non-cyanide bath (Injeti and Leo, 2008). The plating bath contained 10 g/l Zn and 120 g/l NaOH and some commercial brighteners and levelers (Pushpavanam, 2006). Low carbon steel (25 × 50 × 1 mm) was used as substrates, countered by platinum mesh anodes upon deposition. Prior to plating, the samples were soak-cleaned in a 50 °C 50% NaOH solution for 30 mins, electro-cleaned in 5% NaOH at room temperature for another 10 s, and finally dipped in 5% HCl for 10 s. Electrodeposition was carried out at the room temperature using a current density of 2 A/dm² for 30 mins. Subsequently, the samples were cleaned, dried, and mounted in one of the configurations (30 mm O.D.) as presented in Fig. 1 ready for the different surface preparation protocols and characterization techniques. As for the sandwich-mounted samples (Chu and Sheng, 1984), the preparation steps include coupling 2 cross-sectioned samples with their coating layers facing one another, inserting the couple in a copper tube (30 mm O.D.), filling of Gatan glue in the tube, cutting of the specimen to a 200 μm disc, and grinding the disc down to 100 μm.

3.2. Test protocols

3.2.1. Surface preparation

The cross-sectioned samples that were cold mounted were prepared for the SEM specimens by grinding on a rotating disc with abrasive SiC papers with 800–4000 grits and polishing by 1 of the 3 schemes, namely (1) mechanical polishing with an oil-based diamond suspension (3 μm and 1 μm) on a rotating disc, (2) final polishing with a 50% colloidal silica (0.05 μm) slurry in a 50 Hz vibration polishing machine, and (3) final polishing with electrochemical polishing using the Spyridelis' formulation composed of 50% orthophosphoric acid in ethyl alcohol with 3 V and current density of 2 A/dm² at room temperature for 5–20 s (Spyridelis,

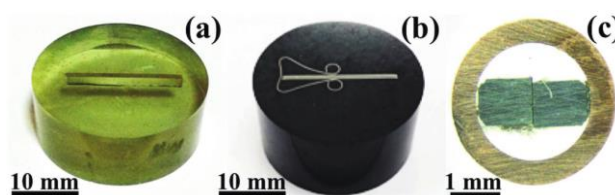


Fig. 1. Mounting methods of the studied specimens in the current study: (a) cold mounting for SEM specimens; (b) hot-mounting using electrically conductive powder for EBSD specimens, and (c) sandwich-mounting for EBSD and TEM specimens to be electrochemically polished.

Table 1
Surface preparation methods of the specimens in the current study.

Sample name	Surface finishing process	Polishing mediums
SEM-1	Mechanical Polishing	Diamond suspension 1 μm
SEM-2	Vibrational Polishing	Colloidal silica 0.05 μm
SEM-3	Electrochemical Polishing	Spyridelis's method
EBS-1	Vibrational Polishing	Colloidal silica 0.05 μm
EBS-2	Electrochemical Polishing	Adair's method
TEM-1	Electrochemical Polishing	Spyridelis's method
TEM-2	Electrochemical Polishing	Adair's method

1971). The electrochemical polishing process was performed with an automatic twin-jet electropolisher (Fischione, model 120) with controlled electrolytic flow and electrical potential. These specimens will be termed SEM-1, SEM-2, and SEM-3, respectively.

The cross-sectioned samples that were hot mounted using conductive powder were subsequently prepared for EBSD-1 specimens by grinding and polishing with a 50% colloidal silica solution as above. On the other hand, the sandwich-mounted samples were electrochemically polished using the Adair's formulation composed of 20% perchloric acid in ethanol with 18 V at room temperature for 5–20 s (Edington, 1975). This second set of EBSD specimens is termed EBSD-2. Finally, the TEM specimens were prepared from the sandwich-mounted samples employing the Spyridelis' and Adair's electrochemical polishing methods. These specimens will be termed TEM-1 and TEM-2, respectively. The surface preparation methods of the specimens of various sets are summarized in Table 1.

3.2.2. Characterization

The SEM examination was performed under a field emission scanning electron microscope (SU8030Hitachi) with 10 kV, and the SEM micrographs were collected in the secondary electron mode. The EBSD examination was performed with a scanning electron microscope equipped with EBSD mode (S3400N Hitachi) with 20 kV, 90 mA, tilt angle 70°, scan rate 12.6 points/second. A transmission electron microscope (JEOL JEM-2010) was employed for the TEM examination.

4. Results and discussion

4.1. Surface finishing for metallography

4.1.1. SEM

All electrogalvanized specimens with approximately 15 μm coating thickness were successfully prepared and exhibited uniform coating structures, comprising of sub-micron nodules as observed on the top surface (Fig. 2(a)). Following cross-sectioning, grinding and polishing using different sample preparation protocols, distinct surface characteristics were obtained, as shown in Fig. 2(b–d). By utilizing oil-based diamond suspension as polishing medium (SEM-1), cross-sectional surface of the specimen becomes well-leveled and uniform generally. However, microstructural fea-

tures of the coating were not clearly exposed. This demonstrates that the oil-based diamond suspension was adequate for surface polishing of electrogalvanized coating, but without an observable etching effect.

With an addition of the colloidal silica polishing step (SEM-2), the microstructural features of the coating remained not clearly seen, albeit the polished surface is uniform and defect-free. Furthermore, the entire zinc layer appears to be eroded with respect to the steel substrate. A similar response of uniform removal of polished surfaces has been observed in other metals polished with colloidal silica, and the synergic effects of mechanical abrasion and chemical etching was noted to be the main causes (Jiang et al., 2015).

Replacing the colloidal silica final polishing with electrochemical polishing of Spyridelis method, a columnar-grain structure of the galvanized coating becomes clearly visible under the SEM with measurable columnar size of 1–2 μm , as evidenced in Fig. 2(d). Furthermore, the polished surface is generally uniform and exhibits a good level of flatness with respect to the substrate layer. Typically, in the electro-chemical polishing process, an acidic solution accompanied by anodic currents develops thin polish film on the surface of the specimen, which enables uniform polishing that well minimizes refined peaks and valleys of the surface. At the relatively low voltage (3–5 V) and low current (1–3 A/dm²), the etching effect is predominant allowing specific dissolution of the more loosely-bound atoms at the grain boundaries (Vander Voort, 1999). It appears that the Spyridelis electropolishing method with 5 s polishing period comprises suitable electro-chemical formulation and protocol that allow simultaneous polishing and etching of electrogalvanized surface in a controlled manner without rapid attack on the in-grain areas, leading to appreciable quality of the etched surface.

4.1.2. EBSD

Specimens EBSD-1 and EBSD-2 were prepared by mechanical polishing with colloidal silica and electro-chemical polishing using Adair method, respectively. As also learned from specimen SEM-2 which has the similar sample preparation protocol, mechanical polishing with colloidal silica provides EBSD-1 with a uniformly polished galvanized surface, but with negligible etching effects and non-leveling at the coating interface. When closely examined under EBSD, the galvanized layer was found to exhibit some roughness and non-uniformity (Fig. 3(a)). Mechanical polishing with colloidal silica therefore does not provide adequate polishing quality for EBSD examination.

Fig. 4 shows the development of the polished surfaces of the EBSD-2 specimens over different periods of electro-chemical polishing sessions (5–20 s). Increasing a polishing duration, the polished surfaces were progressively refined and flatten. 5 s was found as the optimum polishing time. Under the EBSD, the specimen exhibited highly uniform and flat surface across the galvanized and steel layers (Fig. 3(b)). Furthermore, some small degree of etching on the specimen's surface is evidenced. These characteristics

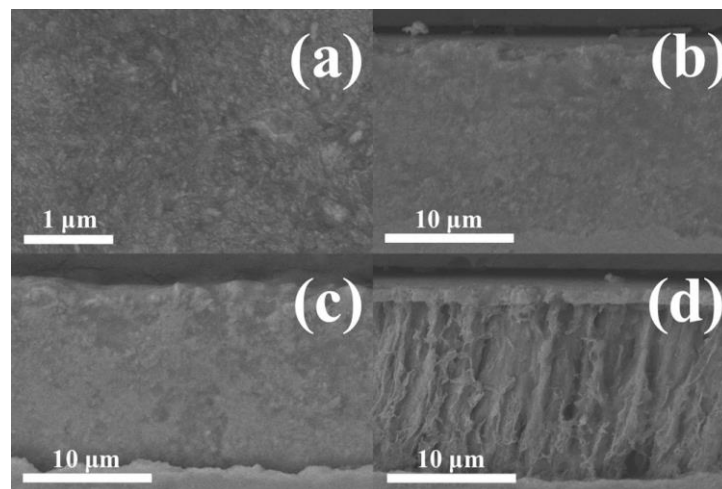


Fig. 2. SEM micrographs presenting (a) a top-view surface of electrogalvanized sample and cross-sectional surfaces of specimens (b) SEM-1, (c) SEM-2, and (d) SEM-3 following their final polishing step.

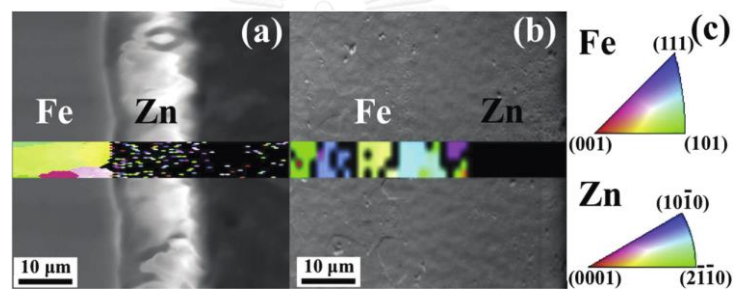


Fig. 3. EBSD micrographs showing cross-sectional surfaces and crystal orientation mapping of specimens (a) EBSD-1 and (b) EBSD-2. The references of crystal orientation is presented in (c).

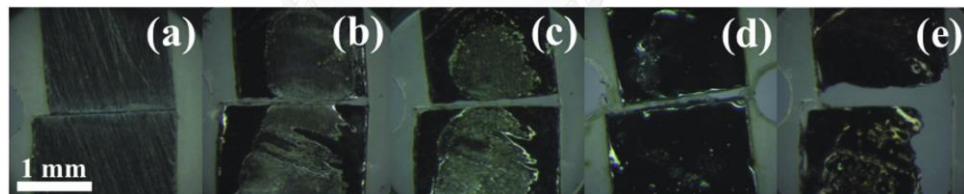


Fig. 4. The sandwich-mounted samples (specimens EBSD-2) undergone electrochemical polishing sessions utilizing Adair's method for different polishing durations: (a) 0, (b) 5, (c) 10, (d) 15, and (e) 20 s.

are desirable for EBSD examination, and thus the Adair's electrochemical polishing method appears to be suitable for the analysis. It should be noted however that only the areas of iron were identified in the phase mapping of the two groups of specimens. This should be owed to the grain sizes of zinc, which are somewhat below the resolution of the LaB₆ crystal-equipped EBSD instrument being employed (50–100 nm).

4.2. Sample thinning for TEM

The electrogalvanized specimens were prepared to the mounted units as exemplified in Fig. 5, and grinding and electro-chemical polishing sessions were subsequently conducted. A relatively long polishing time of 15 s was found to be the optimum for each polishing condition. Using the Spyridelis's electro-chemical polishing protocol, the surfaces of TEM-1 specimen remained visually blunt

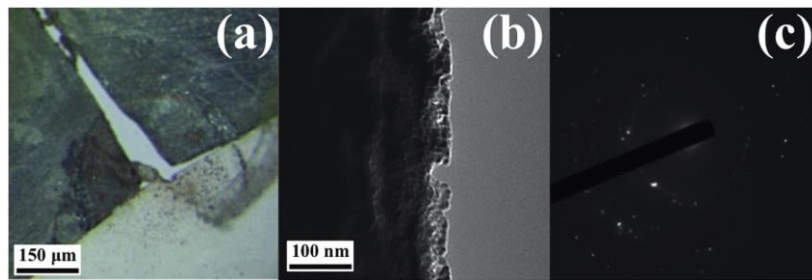


Fig. 5. The image of specimen TEM-1 electrochemically polished with Spyridelis's method, TEM bright field micrograph and corresponding diffraction patterns of the selected area.

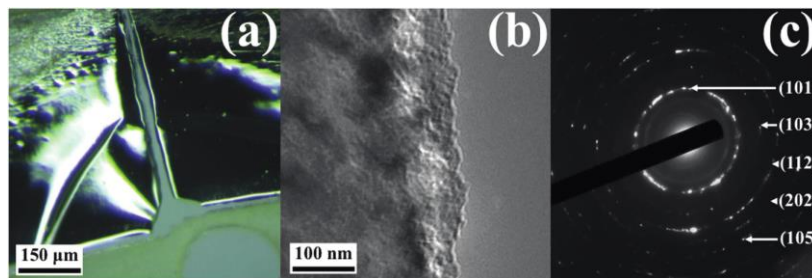


Fig. 6. The image of specimen TEM-2 electrochemically polished with Adair's method, TEM bright field micrograph and corresponding diffraction patterns of the selected area.

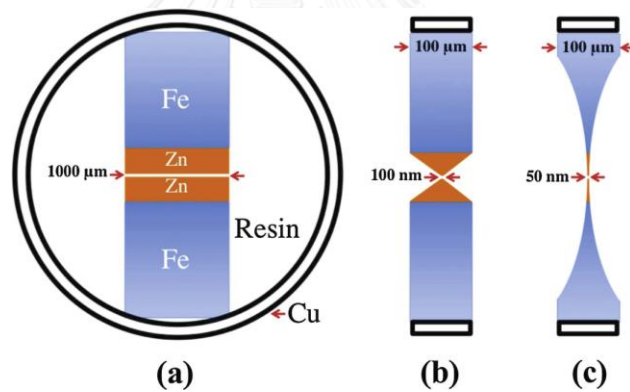


Fig. 7. Schematic illustrations of the sandwich-mounted samples: (a) cross section of the as-mounted; and side-views of the specimens after electrochemical polishing method of (b) Spyridelis's and (c) Adair's.

and rough, as presented in Fig. 5(a). This is echoed by the presence of the dark and non-distinguishable areas in the bright field micrograph (Fig. 5(b)) and the obscure spots in the diffraction patterns (Fig. 5(c)). These qualities clearly prevent legitimate TEM analysis of the electrogalvanized specimens.

On the other hand, the use of the Adair's electro-chemical protocol in specimen TEM-2 yielded highly flat and shiny surfaces, as shown in Fig. 6(a). When examined under the TEM, semi-transparent areas that exposed microstructural details could be

observed from surfaces of specimens (Fig. 6(b)). Furthermore, the obtained diffraction patterns are characterized by a series of distinct spots (Fig. 6(c)), which allow clear identifications of the crystallographic structure and orientations of coating. The crystallographic planes of (103), (112), (202), (105), and the dominant (101) are determined for this system. Thus, the Adair's method performs far better than the Spyridelis in this regard. This can be rationalized from a schematic diagram in Fig. 7. Whereas the galvanized coating was preferentially etched in the Spyridelis protocol

resulting in a blunt tip with a moderate tip size of about 100 nm, the Adair's procedure allowed simultaneous etching of both steel and zinc in a stable and controlled manner, and a needle-shaped tip of about 50 nm width could then be realized. The sample configuration as shown in Fig. 7(c) is a typical form that provides the TEM analysis of distinguished quality as has been obtained during the examinations of other classes of metals (Mogensen and Glejbold, 1992; Michalcová et al., 2013; Dawson and Tatlock, 2015; Ünlü, 2008).

Conclusions

The present study has demonstrated the challenges and strategies of surface modification of electrogalvanized coatings for electron microscopy analysis. To prepare the surface of electrogalvanized coating for microstructural examinations under the SEM, electrochemical polishing with the Spyridelis' method was found superior over the typical mechanical polishing routes that utilize oil-based diamond suspension or colloidal silica, as it provided simultaneous polishing and etching of electrogalvanized surface in a controlled manner without rapid attack on the grain interiors. On the other hand, the electrochemical polishing with Adair's method appeared to the EBSD examinations of electrogalvanized specimens, as it allowed gradual polishing of both zinc coatings and steel substrates with adequate etching effects. Such unique characteristic of the Adair's method was also found effective for preparing exceptionally thin and uniform electrogalvanized specimens for TEM analysis

Acknowledgements

The financial support from the Thailand Research Fund through the Royal Golden Jubilee Ph.D. Program (PHD/0086/2554), and the grant for the Surface Coatings Technology for Metals and Materials Research Unit (GRU 57-005-62-001) and the grant for International Research Integration: Chula Research Scholar (GCRS.58.02.21.01), Ratchadaphiseksomphot Endowment Fund, are gratefully acknowledged.

References

- Aliya, D., 2004. Metallographic sectioning and specimen extraction. *Metallography and microstructures*. *ASM Int.* 9, 229–241.
- Chianpairot, A., Lothongkum, G., Schuh, C.A., Boonyongmaneerat, Y., 2011. Corrosion of nanocrystalline Ni-W alloys in alkaline and acidic 3.5 wt.% NaCl solutions. *Corros. Sci.* 53, 1066–1071.
- Chu, S.N.G., Sheng, T.T., 1984. TEM cross section sample preparation technique for III-V compound semiconductor device materials by chemical thinning. *J. Electrochem. Soc.* 131 (11), 2663–2667.
- Crotty, D., 1996. Zinc alloy plating for the automotive industry. *Met. Finish.* 94, 54–58.
- Dawson, K., Tatlock, G.J., 2015. Preparation of micro-foils for TEM/STEM analysis from metallic powders. *Micron* 74, 54–58.
- Edington, J.W., 1975. Practical electron microscopy in materials science. In: *Electron Diffraction in the Electron Microscope*, 2nd ed. Macmillan Press, pp. 122.
- Eppensteiner, F.W., Jennkind, M.R., 2007. Chromate conversion coatings. *Met. Finish.*, 413–424.
- Exner, H.E., Weinbruch, S., 2004. Scanning electron microscopy, metallography and microstructures. *ASM Int.* 9, 355–367.
- Injeti, G., Leo, B., 2008. Electrodeposition of nanostructured coatings and their characterization—a review. *Sci. Technol. Adv. Mater.* 9, 1–11.
- Jiang, L., He, Y., Luo, J., 2015. Chemical mechanical polishing of steel substrate using colloidal silica-based slurries. *Appl. Surf. Sci.* 330, 487–495.
- Marder, A.R., 2000. The metallurgy of zinc-coated steel. *Prog. Mater. Sci.* 45, 191–200.
- Michalcová, A., Vojtech, D., Novák, P., 2013. Selective aluminum dissolution as a means to observe the microstructure of nanocrystalline intermetallic phases from Al-Fe-Cr-Ti-Ce rapidly solidified alloy. *Micron* 45, 55–58.
- Mogensen, K.E., Glejbold, K., 1992. Preparation of TEM specimens from a hardened tool steel. *Micron Microsc. Acta* 23, 199–200.
- Morales, J., Díaz, F., Hernández-Borges, J., González, S., Cano, V., 2007. Atmospheric corrosion in subtropical areas: statistic study of the corrosion of zinc plates exposed to several atmospheres in the province of Santa Cruz de Tenerife (Canary Islands, Spain). *Corros. Sci.* 49, 526–541.
- Muralidhara, H.B., Arthoba Naik, Y., 2008. Studies on nanocrystalline zinc coating. *B. Mater. Sci.* 31, 585–591.
- Muster, T.H., Cole, I.S., 2004. The protective nature of passivation films on zinc: surface charge. *Corros. Sci.* 46, 2319–2335.
- Pushpavanam, M., 2006. Role of additives in bright zinc deposition from cyanide free alkaline baths. *J. Appl. Electrochem.* 36, 315–322.
- Raeissi, K., Saatchi, A., Golozar, M.A., Szpunar, J.A., 2007. Effect of surface preparation on zinc electrodeposited texture. *Surf. Coat. Technol.* 197, 229–237.
- Ramanauskas, R., Quintana, P., Maldonado, L., Pomés, R., Pech-Canul, M.A., 1997. Corrosion resistance and microstructure of electrodeposited Zn and Zn alloy coatings. *Corros. Sci.* 39, 16–21.
- Ramanauskas, R., Gudavičiūtė, L., Juškėnas, R., Ščit, O., 2007. Structural and corrosion characterization of pulse plated nanocrystalline zinc coatings. *Electrochim. Acta* 53, 1801–1811.
- Reimer, L., 2013. *Transmission Electron Microscopy: Physics of Image Formation and Microanalysis*. Springer, pp. 36.
- Saber, K., Koch, C.C., Fedkiw, P.S., 2003. Pulse current electrodeposition of nanocrystalline zinc. *Mater. Sci. Eng. A Struct.* 341, 174–181.
- Samuels, L.E., 2003. Metallographic polishing by mechanical methods. *ASM Int.* 9, 257–280.
- Spyridelis, J., 1971. Dislocation loops and stacking faults in zinc. *Mater. Res. Bull.* 6, 1345–1352.
- Ünlü, N., 2008. Preparation of high quality Al TEM specimens via a double-jet electropolishing technique. *Mater. Charact.* 59 (5), 547–553.
- Vander Voort, G.F., 1984. *Metallography: Principles and Practice*. McGraw-Hill, in: *ASM INT* 9 1999, 281–293.
- Venables, J.A., Harland, C.J., 1973. Electron back-scattering patterns—a new technique for obtaining crystallographic information in the scanning electron microscope. *Philos. Mag.* 27 (5), 1193–1200.
- Wang, R.Y., Kirk, D.W., Zhang, G.X., 2006. Effects of deposition conditions on the morphology of zinc deposits from alkaline zincate solutions. *Electrochem. Soc.* 153, C357–C364.
- Weidmann, E., 1985. Electrolytic polishing, metallography and microstructures. *Am. Soc. Mater.* 9, 48–56.
- Wilcox, G.D., Gabe, D.R., 1993. Electrodeposited zinc alloy coatings. *Corros. Sci.* 35, 251–258.
- Winand, R., 1991. Electrocrystallization: fundamental considerations and application to high current density continuous steel sheet plating. *J. Appl. Electrochem.* 21, 377–385.
- Yoshioka, K., Watanabe, K., Kato, Y., 1990. Process for electroplating stainless steel strips with zinc or zinc-nickel alloy. U.S. PAT. US4969980 A.
- Zhang, X., Van den Bos, C., Sloof, W.G., Hovestad, A., Terry, H., de Wit, J.H.W., 2005. Comparison of the morphology and corrosion performance of Cr(VI)- and Cr(III)-based conversion coatings on zinc. *Surf. Coat. Technol.* 199, 92–104.
- Zhang, G.A., Yu, N., Yang, L.Y., Guo, X.P., 2014. Galvanic corrosion behavior of deposit-covered and uncovered carbon steel. *Corros. Sci.* 86, 202–212.

OUTPUT

Publications:

Paper 1 Narin Jantaping, Chaiyasit Banjongprasert, Torranin Chairuangstri, Ussadawut Patakham, Yutthanant Boonyongmaneerat, "Challenges and strategies of surface modification of electrogalvanized coatings for electron microscopy analysis," *Micron*, vol. 86, pp. 48-53, 7 (2016).

Paper 2 submitted to *Surface & Coatings Technology* journal with the title of Influences of texture and nanostructural features on corrosion properties of electrogalvanized coatings and passivation layers, Narin Jantaping, Christopher A. Schuh, and Yuttanant Boonyongmaneerat, May 10, 2017.

Conferences:

1. Narin Jantaping, Christopher A. Schuh, Shiahn Chen, Yuttanant Boonyongmaneerat, "Influences of Nanostructural Features on Corrosion Properties of Electrogalvanized Coatings," Materials Research Society (MRS), Boston, MA, USA, November 27-December 2, 2016 (Poster presentation)
2. Narin Jantaping, Chaiyasit Banjongprasert, Torranin Chairuangstri, Christopher A. Schuh, Yutthanant Boonyongmaneerat, "Metallography Techniques for Microscopy of Electrogalvanized Coatings: Effectiveness of Mechanical, Electrochemical, and Ion

polishing,” 11th Asia-Pacific Microscopy Conference (APMC11), Phuket, Thailand, May 23 to 27, 2016 (Oral presentation)

3. Narin Jantaping, Chaiyasit Banjongprasert, Torranin Chairuangri, Ussadawut Patakham, Yutthanant Boonyongmaneerat, “Challenges and Strategies in Characterizing Electrodeposited Zinc Coatings via Electron Microscopy Techniques,” 10th International Conference on the Physical Properties and Application of Advanced Materials (ICPMAT2015), November 17-21, 2015 (Oral presentation)

4. Narin Jantaping and Yuttanant Boonyongmaneerat, “Graphene-based coatings,” Joint workshops of Nanyang Technological University and Chulalongkorn University on Nanoscience and Technology,” Singapore, September 11 – 12, 2014 (Poster presentation)

5. Narin Jantaping, Christopher A. Schuh, and, Yuttanant Boonyongmaneerat, “Influences of texture and nanostructural features on corrosion properties of electrogalvanized coatings and passivation layers,” RGJ-PHD Congress 18, Nonthaburi, Thailand June 8-10, 2017 (Oral presentation)

VITA

Acting Sub Lt. Narin Jantaping

Date of Birth: May 19, 1984

Home Address: 17/4, Moo.4, Rimping, Maung, Lamphun 51000, Thailand

Institution Address: Nanoscience and Technology, International Program, Chulalongkorn University, Room 1106, Metallurgy and Materials Science Research Institute Building, Soi Chula 12, Phyathai Road, Pathumwan, Bangkok 10330, Thailand, Tel: +6622184231, Fax: +6622184231

Education:

2012 – Present: Ph.D. Candidate in Nanoscience and Technology, International Program, Graduate School, Chulalongkorn University, Bangkok, Thailand.

2003 – 2006: B.S. Materials Science, Department of Physics and Materials Science, Faculty of Science, Chiang Mai University, Chiang Mai, Thailand.

Scholarship:

2012 – Present: The Royal Golden Jubilee Ph.D. Program, The Thailand Research Fund. And The Center of Innovative Nanotechnology, Chulalongkorn University

Research Interests: Nanoscience and technology, Electrodeposition process, Materials for anti-corrosion coating technology, X-ray analysis and electron microscopy of materials.

Work and Research Experience:

2015: Research experience at Department of Materials Science and Engineering, Massachusetts Institute of Technology (MIT), USA.

2012 – Present: Research Assistant, The Royal Golden Jubilee Ph.D. Program.

2007 – 2012: Work experience on the X-ray techniques laboratory officer, Materials Characterization Research Unit, National Metal and Materials Technology Center (MTEC).

2006: Undergraduate Research Assistant, National Metal and Materials Technology Center (MTEC).

